ROYAL SOCIETY
OF CHEMISTRY

Check for updates

Injectable self-healing oxidized pectin and carbohydrazide-modified gelatin hydrogels for curcumin-loaded zein nanoparticle delivery in antioxidant therapy

Francesca Tivano, [ID] [a,b,c] Elena Marcello, [ID] [a,b,c] Camilla Paoletti, [ID] [a,b,c] Alice Zoso, [ID] [a,b,c] Clara Mattu, [ID] [a,b,c] Irene Carmagnola [ID] †[a,b,c] and Valeria Chiono [ID] *†[a,b,c]

The design of drug delivery systems (DDS) for efficient and sustained *in situ* antioxidant treatment is demanded in regenerative medicine applications. DDS, based on nanoparticle-loaded hydrogels, are promising advanced drug delivery platforms to achieve prolonged release and targeted bioactivity. Herein we developed innovative and sustainable injectable hydrogels based on oxidized pectin (PDA) and carbohydrazide-modified gelatin (G-CDH) for the release of curcumin-loaded zein nanoparticles (CurZNPs) for mitigating cell oxidative stress. CurZNPs, produced by nanoprecipitation, exhibited high encapsulation efficiency, sustained curcumin release, and strong antioxidant and anti-inflammatory activities. PDA/G-CDH hydrogels with three different PDA : G-CDH ratios were prepared by double physical and chemical crosslinking, through calcium ions internally released from $CaCO_3$ and Schiff base formation between PDA and G-CDH functional groups, respectively. PDA/G-CDH hydrogels showed rheological tunability, depending on the degree of pectin oxidation (2.5 mol%: PDA_2.5 and 5 mol%: PDA_5). Hydrogels with a balanced aldehyde-to-amine ratio, specifically the PDA_2.5/G-CDH (70 : 30) and PDA_5/G-CDH (50 : 50) formulations, were selected based on their superior stability in physiological conditions, consistent with effective crosslinking. Such compositions also exhibited injectability through shear thinning behaviour, and self-healing by restored mechanical integrity after stress, and supported human fibroblast viability and attachment. CurZNPs-loaded PDA/G-CDH hydrogels showed prolonged curcumin release, antioxidant activity by restoring fibroblast viability after induced oxidative damage, and anti-inflammatory properties with RAW 264.7 macrophages. In conclusion, injectable PDA/G-CDH hydrogels were efficient and biocompatible DDS for antioxidant treatment through controlled CurZNPs release.

1   Introduction

Oxidative stress has been identified as a critical factor hindering regeneration in various pathological conditions.[1] Imbalance between oxidant and antioxidant species leads to the accumulation of reactive oxygen species (ROS), disrupting molecular and redox cell signaling.[2] While low ROS levels support normal healing by promoting immune cell recruitment and tissue repair, excessive ROS accumulation impairs essential cellular processes, prolonging inflammation.[3]

[a]Department of Mechanical and Aerospace Engineering, Politecnico di Torino, Torino, Italy. E-mail: valeria.chiono@polito.it
[b]POLITO BioMedLab, Politecnico di Torino, Torino, Italy
[c]Interuniversity Center for the Promotion of the 3Rs Principles in Teaching and Research, Italy
† These authors contributed equally to this study.

Therefore, antioxidant therapies, able to prevent excessive ROS production or inhibit downstream signaling that promotes inflammation or cell death, are currently being investigated to enhance healing.[4] Emerging antioxidant therapeutic strategies include the use of plant-derived biomolecules, able to support the natural repair mechanisms, by mitigating oxidative damage, thus offering the potential for improved treatments.[5,6] Among them, curcumin (from plants of the *Curcuma longa* species) is a natural antioxidant agent that has been reported to reduce oxidative stress in several clinical applications.[7,8] Curcumin can scavenge excessive ROS, relieving cellular and tissue harm caused by oxidative stress and enhancing healing.[9] However, curcumin efficiency is limited by its hydrophobic nature with low solubility in aqueous solutions (~20 µg mL^{-1}) and poor bioavailability at physiological pH.[10] Moreover, despite its therapeutic potential, curcumin is also affected by dose-dependent toxicity: at high concen-

trations, it can cause mitochondrial dysfunction leading to cell apoptosis.[11] Its therapeutic effect can be improved through encapsulation into drug delivery systems (DDSs) specifically designed to extend curcumin half-life, increase bioavailability, provide controlled release to mitigate toxicity risks and extend efficiency. Advanced DDSs based on curcumin-loaded nanoparticles (NPs) embedded into hydrogels are particularly promising:[12] the hydrophilic polymer network of hydrogels provides an injectable depot for localized and sustained drug delivery minimizing burst release, whereas NPs allow effective encapsulation, improved drug stability and potential cell-targeting.[12,13]

However, further attention should be given to the sustainability of the materials and production methods used to develop these DDS systems, as current approaches often fall short of fully addressing the need for green hybrid DDSs. Biomaterials should be properly selected to prepare such advanced DDSs. Zein, the main protein of corn, is promising for drug release as it is biocompatible, biodegradable and obtained from agricultural waste.[14,15] Zein has been widely investigated to prepare NPs for the delivery of lipophilic drugs, including curcumin,[16] due to the availability and low -cost of the raw material, and improved biocompatibility of zein over synthetic polymer NPs.[17] Zein NPs encapsulating curcumin have been primarily studied in the food industry for the delivery of nutrient components and dietary supplements, and in pharmaceutical applications as effective oral drug delivery systems.[18,19] However, the potential of zein NPs for antioxidant applications is relatively underexplored.

Pectin, a naturally occurring polysaccharide from citrus fruit peels, offers a sustainable solution to agricultural waste, with millions of tons generated annually.[20,21] Beyond its traditional use as a gelling agent in the food industry,[22,23] its biocompatibility and low cost make it valuable in biomedical applications such as drug delivery and tissue engineering.[24–26] Pectin hydrogels can be easily formed through ionic gelation by crosslinking galacturonic acid groups with divalent cations, using either external or internal crosslinking methods. Internal gelation with $CaCO_3$ ensures the formation of uniform hydrogel networks and decreases pectin acidity, eliminating the need for acidifiers like D-(+)-glucono-1,5-lactone for alginates,[27] increasing biocompatibility.[28] Pectin hydrogels have already shown promising results for the controlled delivery of free curcumin.[29,30] However, pectin-based hydrogels have two drawbacks for their application as *in situ* DDSs: poor *in vivo* biodegradation, due to the absence of enzymes in mammals required for the breakdown of unmodified pectin and the lack of cell-adhesive moieties.[31] To address the first drawback, an oxidized form of pectin (*i.e.*, pectin dialdehyde, PDA) can be obtained by treatment with sodium metaperiodate, leading to a polymer with reduced molecular weight that is able to degrade *via* an alkaline β-elimination mechanism.[32–34] Moreover, pectin aldehyde groups can be used to form chemical crosslinks with gelatin through Schiff base formation: incorporation of gelatin allows the promotion of cell adhesion and proliferation, addressing the other main limitation of pectin. However imine bonds, such as those

formed between PDA and gelatin, are unstable in aqueous environments.[33–35] Previously, carbohydrazide-modified gelatin (G-CDH) has been proposed to form stable hydrazone bonds by reacting with the aldehyde groups of oxidized hyaluronic acid[36,37] and oxidized alginate.[38]

The aim of this study was to develop innovative and sustainable DDSs based on injectable and cell-adhesive pectin-based hydrogels for the delivery of antioxidant zein NPs. PDA/G-CDH hydrogels were prepared by chemical crosslinking *via* Schiff base formation between the aldehyde groups of PDA and the amino and hydrazide groups of G-CDH and physical internal crosslinking through calcium ions released from $CaCO_3$. PDA/G-CDH hydrogels were prepared at different PDA to G-CDH ratios and using PDA with different oxidation degrees, then analyzing their rheological properties, stability and *in vitro* cytocompatibility. The characterization allowed an assessment of their potential as injectable and self-healing hydrogels. In parallel, zein NPs loaded with curcumin (CurZNPs) were prepared and their release profile and antioxidant properties were evaluated. Optimized CurZNPs were incorporated into PDA/G-CDH hydrogels and their release kinetics were studied. The CurZNPs delivered *via* injectable PDA/G-CDH hydrogels reduced the oxidative stress in human fibroblasts by scavenging ROS, showing promise for future soft tissue regenerative applications.

2 Materials and methods

2.1 Materials

Zein was kindly supplied by FloZein Products. Citrus pectin (Classic CU 701 lot. no. 12204320) was purchased from Herbstreith & Fox and kindly supplied by Bio3DPrinting Srl (Cascina, Italy). Sodium metaperiodate, carbohydrazide, N-(3-dimethylaminopropyl)-N′-ethylcarbodiimide hydrochloride (EDC), and 1-hydroxybenzotriazole monohydrate (HOBT) were purchased from Thermo Fisher Scientific. Porcine skin gelatin (type A), curcumin and all other reagents were purchased from Sigma-Aldrich unless specified otherwise.

2.2 Methods

2.2.1 Preparation of curcumin-loaded zein nanoparticles (CurZNPs). Curcumin-loaded zein nanoparticles (CurZNPs) were prepared *via* nanoprecipitation. In detail, zein (10 mg mL^{-1}) and curcumin (2 mg mL^{-1}) stock solutions were dissolved separately in acetone/dH$_2$O solution (60:40% v/v) under dark conditions. Then, stock solutions were diluted in acetone/dH$_2$O solution (60:40% v/v) to reach their final concentrations, *i.e.*, 1–25 mg mL^{-1} for zein and 0.125 mg mL^{-1} for curcumin. Zein/curcumin solution was added dropwise into dH$_2$O (1:5 volume ratio), while stirring at 700 rpm for 30 min at room temperature, under dark conditions.[16] Residual acetone in the nanodispersion was removed by evaporation under a chemical hood for 15 min; then, dH$_2$O was added to replace the volume of evaporated acetone. Zein NPs without curcumin (ZNPs) were prepared as control from zein solution

at 1 mg mL^{-1} final zein concentration in acetone/dH$_2$O solution (60:40% v/v), then following the same steps as for CurZNPs.

2.2.2 Oxidized pectin (PDA) production. Pectin was oxidized with sodium metaperiodate (NaIO$_4$) at two theoretical degrees of oxidation (2.5 and 5%), depending on the weight ratio between pectin and NaIO$_4$.[16,39–41] Pectin (1 g) was dissolved in 5 mL ethanol, and the suspension was stirred for 1 h. Then, different amounts of NaIO$_4$ (Table 1) were dissolved in 5 mL dH$_2$O and added dropwise to the pectin solution to achieve the target degree of oxidation. The solution was allowed to react in the dark, according to Table 1, and then the reaction was quenched in 1 mL ethylene glycol while stirring for 30 min. A starch–potassium iodide (KI) test was employed to quantify the unreacted NaIO$_4$ before quenching the reaction with ethylene glycol.[42] KI was dissolved in dH$_2$O at 20% w/v, covered from light, while starch was dissolved in phosphate buffered saline (PBS) at 1% w/v at 100 °C. A volume of 100 μL of the reacting oxidized pectin solution was added to 24.9 mL dH$_2$O. Then, 300 μL of this solution was added to a solution including: 75 μL starch solution, 75 μL KI solution and 50 μL dH$_2$O. The solution was rapidly vortexed, and then absorbance at 486 nm was measured with a microplate reader (Thermo Scientific™ Varioskan™ LUX Multimode Microplate Reader). The concentration of residual NaIO$_4$ was determined with a calibration curve (0.0016–0.02 mg mL^{-1}).

After quenching, the solution of PDA was then dialyzed against dH$_2$O for at least 5 days (Spectrum™ Spectra/Por™ membrane, with molecular weight cut off: 6000–8000 Da). The starch–KI test was repeated on the dialysis medium, using 10-fold volumes, to verify that all the unreacted NaIO$_4$ had been successfully removed from the PDA. Finally, the material was stored at −20 °C and then freeze-dried.

2.2.3 Carbohydrazide-modified gelatin (G-CDH) synthesis. G-CDH was synthesized following a procedure previously described in the literature.[40] Gelatin (3 g) was dissolved in 300 mL dH$_2$O obtaining a solution with 1% w/v concentration. Carbohydrazide (2.2 g) was added to the above solution during stirring. Then, after 30 min, 10 mL N-(3-dimethylaminopropyl)-N′-ethylcarbodiimide hydrochloride (EDC) solution in dH$_2$O (4.5% w/v) and 10 mL 1-hydroxybenzotriazole monohydrate (HOBT) solution in dimethyl sulfoxide (DMSO, 4.5% w/v) were further added dropwise while stirring. The pH of the final solution was measured and adjusted to 5.25, and the reaction was left to proceed for 19 hours.

Then, the solution was dialyzed (Spectrum™ Spectra/Por™ membrane with 6000–8000 Da molecular weight cut off) against 0.1 M NaCl solution for 3 days, against ethanol/dH$_2$O

solution (10:90% v/v) for 2 days, and dH$_2$O for 2 days. Finally, the material was stored at −20 °C and then freeze-dried.

2.2.4 PDA/G-CDH hydrogel preparation. PDA stock solution (6% w/v) was dissolved in 20 mM NaHCO$_3$ water solution overnight. Two suspensions of CaCO$_3$ powder in PBS with 20 and 30 mM concentrations were prepared. PDA hydrogels pre-crosslinked with CaCO$_3$ suspensions were herein referred to as pre-hydrogels. Pre-hydrogels were prepared by one-step mixing of PDA solution with CaCO$_3$ suspension through Luer-lock double syringes. To get pre-hydrogels with a closer pH to the physiological value, PDA stock solution was mixed with CaCO$_3$ suspensions at 2:1 and 1:1 volume ratios to reach final PDA pre-hydrogel concentrations of 4% and 3% w/v, respectively.[28,31] The pH values were monitored at different time points after CaCO$_3$ addition (5, 10, 20, 30, 45 and 60 min).

After PDA pre-hydrogel optimization, PDA hydrogels were prepared by further applying a two-step double-syringe mixing method. G-CDH stock solution (6% w/v) was dissolved in PBS at 60 °C. The PDA solution pre-mixed with 30 mM CaCO$_3$ suspensions was selected for hydrogel preparation. After 10 min, to allow the Ca^{2+}-driven internal physical crosslinking to occur, the pre-hydrogel was mixed with G-CDH, to obtain the final hydrogels. Hydrogels with a total polymer content of 3% w/v were prepared by varying PDA to G-CDH ratios (30:70, 50:50, and 70:30% w/w), as detailed in Table 2. PDA hydrogels were also formulated using unmodified gelatin in place of G-CDH, as described in the SI.

For in vitro stability tests and biological characterizations, hydrogels were prepared in sterile conditions. PDA powders were sterilized by UV light for 30 minutes on each side under a biological hood. CaCO$_3$ was autoclaved at 121 °C. G-CDH was solubilized and then filtered through a BioFil Syringe Filter with 0.22 μm pore size. Hydrogel preparation was performed under a biological hood.

2.2.5 Injectable PDA/G-CDH hydrogels loaded with CurZNPs. PDA/G-CDH hydrogels were prepared in sterile conditions as described in the section 2.2.4. Sterile CurZNPs were prepared from filtered solutions. A third step was introduced after PDA/G-CDH mixing to load the CurZNPs suspension into the hydrogels. CurZNPs (25 μg mL^{-1} curcumin) were loaded into 100 μL PDA/G-CDH hydrogels by a Luer-lock double-syringe mixing system, at 1:9 volume of PDA/G-CDH hydrogel to CurZNPs suspension.

Table 1 NaIO$_4$ amount and reaction time for different degrees of pectin oxidation, respectively

Degree of pectin oxidation (mol %)	NaIO$_4$ (mg)	Reaction time (h)
2.5	32.1	1
5	64.2	1.5

Table 2 PDA/G-CDH hydrogel compositions

Hydrogel code	PDA oxidation degree (%)	Weight ratio	
		PDA	G-CDH
PDA_2.5/G-CDH (30:70)	2.5	30	70
PDA_2.5/G-CDH (50:50)	2.5	50	50
PDA_2.5/G-CDH (70:30)	2.5	70	30
PDA_5/G-CDH (30:70)	5	30	70
PDA_5/G-CDH (50:50)	5	50	50
PDA_5/G-CDH (70:30)	5	70	30

2.3 CurZNPs characterization

2.3.1 Size, surface charge and yield. Size, polydispersity index (PDI) and zeta potential were measured using a dynamic light scattering (DLS) instrument (Litesizer™ 500, Anton Paar). All measurements were conducted in triplicate and repeated three times. The yield of the process was measured after 24 hour freeze-drying of prepared CurZNPs using eqn (1):

$$\mathrm{Yield_{CurZNPs}}(\%) = \frac{\text{freeze-dried CurZNPs (mg)}}{\text{inital zein and curcumin (mg)}} \times 100 \quad (1)$$

2.3.2 Encapsulation efficiency and release studies. Curcumin encapsulation efficiency (EE) was evaluated from freshly prepared CurZNPs. CurZNPs were centrifuged at 15 000 rpm for 15 min at room temperature, supernatants were collected and the absorbance was measured at 425 nm with a microplate reader (Thermo Scientific™ Varioskan™ LUX Multimode Microplate Reader). The calibration curve was measured with curcumin in ethanol at different concentrations (0.1–100 µg mL^{-1}). The percentage of loaded curcumin (EE) was calculated by eqn (2):

$$\mathrm{EE}\,(\%) = \frac{\text{initial curcumin (µg mL}^{-1}) - \text{detected curcumin (µg mL}^{-1})}{\text{initial curcumin (µg mL}^{-1})} \times 100 \quad (2)$$

Curcumin release from CurZNPs was evaluated for over 10 days at 37 °C in PBS at physiological (pH 7.4) and acidic pH (pH 4.8). At specific time points (1, 3 and 6 h; 1, 2, 7 and 10 days), samples were centrifuged (15 000 rpm, 15 min at room temperature), supernatants were collected and the absorbance was measured at 425 nm. The amount of released curcumin was determined by eqn (3):

$$\text{Release}\,(\%) = \frac{\text{detected curcumin (µg)}}{\text{initial amount of curcumin (µg)}} \times 100 \quad (3)$$

2.3.3 Antioxidant studies. The scavenging activity of CurZNPs for 2,2-diphenyl-1-picrylhydrazyl (DPPH) was evaluated.[43] Different concentrations of free curcumin and CurZNPs (1, 2.5, 3.5, 5, 10 µg mL^{-1}) were prepared in absolute ethanol and dH$_2$O, respectively. A volume of 100 µL of each solution was added to 100 µL of DPPH solution (0.1 µM in ethanol), and then incubated at room temperature under dark conditions for 30 min. The absorbance was measured at 517 nm with a microplate reader (Thermo Scientific™ Varioskan™ LUX Multimode Microplate Reader). The concentration of each sample needed to achieve 50% of scavenging activity (SC$_{50}$) was determined. DPPH in ethanol and DPPH in dH$_2$O were used as blanks for free curcumin and CurZNPs, respectively. Ascorbic acid and empty ZNPs were used as controls.

2.3.4 *In vitro* anti-inflammatory evaluations. RAW 264.7 cells (American Type Culture Collection, ATCC) were maintained in DMEM High Glucose (Gibco) supplemented with 10% FBS, 1% penicillin–streptomycin, and 2% ʟ-glutamine. Cells were maintained at 37 °C in a humidified atmosphere, with 5% CO$_2$.

To determine the CurZNPs' cytocompatibility, RAW 264.7 cells were seeded in 96-well plates (8 × 10^3 cells per well) for 24 h. Then, cells were treated with CurZNPs at different equivalent curcumin concentrations (2.5, 5, and 10 µg mL^{-1}) for 24 h. Cell viability was measured using CellTiter-Blue viability assay, with untreated cells considered as the control group.

To induce the M1 macrophage phenotype switch, the optimal LPS concentration was determined. RAW 264.7 were seeded in 96-well plates (8 × 10^3 cells per well) for 48 h, and cells were treated with LPS at two concentrations (0.05 and 1 µg mL^{-1}) for 24 h. Then, the quantification of nitric oxide (NO) was determined by the Griess test (Promega). For NO quantification, 50 µL of each sample was harvested and combined with an equal volume of Griess reagent according to the manufacturer's instructions. Untreated cells were considered control groups. NO production was evaluated after 5 min incubation in terms of absorbance measured by a microplate reader at 540 nm. The percentage of NO production was calculated according to eqn (4):

$$\text{NO production}\,(\%) = \frac{\text{NO (µg mL}^{-1}) \text{ sample}}{\text{NO (µg mL}^{-1}) \text{ positive control}} \times 100 \quad (4)$$

Finally, the anti-inflammatory activity of CurZNPs was evaluated. RAW 264.7 were seeded in 96-well plates (8 × 10^3 cells per well) for 48 h. Then, cells were treated with CurZNPs (curcumin concentration of 5 µg mL^{-1}) and LPS (1 µg mL^{-1}) for 24 h. Treatment with only LPS was used as positive control. The Griess test was performed, and the percentage of NO production was calculated according to eqn (4).

The anti-inflammatory activity of CurZNPs was also evaluated by immunofluorescence analyses. RAW 264.7 cells were seeded in µ-Slide 18 Well Glass Bottom (Ibidi) at 8 × 10^3 cells per well for 48 h. Then, cells were treated with CurZNPs (curcumin concentration of 5 µg mL^{-1}) and LPS (1 µg mL^{-1}) for 24 h. After 24 h, the cells were fixed in 4% w/v paraformaldehyde (Thermo Fisher Scientific) in PBS for 15 min and subsequently washed with PBS. Cells were permeabilized with Triton X-100 0.5% v/v in PBS for 10 min. RAW 264.7 were then blocked with 1% BSA in PBS for 30 min, followed by incubation with anti-CD86 antibody (ImmunoTools) in 0.1% w/v BSA for 1 h. After washing the cells with PBS, the RAW 264.7 were incubated with secondary antibody anti-rat Alexa Fluor 488 (Life Technologies) and Alexa Fluor 647 Phalloidin staining (Life Technologies) for F-actin, while cell nuclei were counterstained with 4′,6-diamidino-2-phenylindole (DAPI). Samples were imaged using the Nikon Ti2-E fluorescence microscope. Merging was performed using ImageJ (Fiji) software. Moreover, immunofluorescence signal quantification for CD86 was performed to determine the percentage of CD86-positive cells. Six different images for each sample were processed through ImageJ software. For each analyzed image, the estimated fluorescence intensity was normalized with respect to the number of cell nuclei.

2.4 PDA and G-CDH characterization

2.4.1 Yield of production. PDA and G-CDH yields of production were measured by the ratio between the weight of PDA or G-CDH after freeze-drying and the weight of pectin or gelatin powder before oxidation, respectively. The yield of the modification process product was expressed as a percentage by eqn (5):

$$\text{Yield}_{\text{PDA or G-CDH}} (\%) = \frac{\text{freeze-dried polymer}_{\text{PDA or G-CDH}}(\text{mg})}{\text{initial polymer}_{\text{pectin or gelatin}}(\text{mg})} \times 100 \quad (5)$$

2.4.2 Fourier-transform infrared spectroscopy (FTIR). PDA was analyzed by attenuated total reflectance-infrared spectroscopy (ATR-FTIR). The ATR-FTIR spectra were acquired in absorbance mode from unmodified pectin powder and samples of freeze-dried PDA. The samples were analyzed by a Thermo Scientific Nicolet iS50 FTIR Spectrometer (Milano, Italy) equipped with a diamond crystal ATR accessory spectrometer and the data were acquired by OMNIC Paradigm Software, reporting the spectra in the range of 4000–400 cm^{-1} wavenumber with a resolution of 4 cm^{-1} using 32 scans per sample.

2.4.3 Viscosimeter analysis. The intrinsic viscosity of pure pectin and PDA was measured using a Ubbelohde viscosimeter.[32] All the solutions were prepared employing 0.1 M NaCl as solvent and 25 ± 0.4 °C temperature was maintained for all measurements. Pectin and PDA solutions were analyzed at concentrations of 0.025, 0.05, 0.10, 0.15 and 0.20% w/v for pectin, 0.2–0.3–0.4–0.5% w/v for PDA_2.5, PDA_5, and PDA_10 and 0.4–0.6–0.8–1% w/v for PDA_25 according to predictions (data not shown). The flowing times of polymer solutions through the capillary are proportional to their viscosity (η) according to Poiseuille's law. Inherent and reduced viscosity were calculated and plotted against concentration. The intrinsic viscosity of the polymer is related to its molecular weight (M_v) through the Mark–Houwink–Sakurada equation (eqn (6)):[44]

$$[\eta] = K \times M_v{}^{\alpha} \Rightarrow M_v = \sqrt[\alpha]{\frac{[\eta]}{K}} \quad (6)$$

where $K = 0.00014$ and $\alpha = 1.34$ are temperature- and solvent-dependent parameters, given by the producer.

2.4.4 Degree of functionalization by 2,4,6-trinitrobenzenesulfonic acid assay (TNBS). The degree of oxidation of PDA was investigated through the quantification of aldehyde group modification using the 2,4,6-trinitrobenzenesulfonic acid assay (TNBS).[37] Unmodified pectin and PDA were dissolved in dH_2O at 1% w/v. Pectin and PDA solutions (25 μL) were mixed with 25 μL of 30 mM *tert*-butyl carbazate (*t*-BC) solution (1% w/v trichloroacetic acid) and left to react at room temperature for 24 h. After 24 h, 0.5 mL of 6 mM TNBS solution (0.1 M $NaHCO_3$) was added. After 1 h, the reaction was stopped by the addition of 0.55 mL of 0.5 N HCl and the absorbance was analyzed at 340 nm using a microplate reader. The calibration curve was calculated analyzing standard solutions at known concentrations of *t*-BC (5–30 mM). The degree of oxidation of pectin was obtained by eqn (7):

$$\text{Degree of oxidation} (\%) = \frac{\text{aldehyde groups (mmol)}}{\text{galacturonic acid units (mmol)}} \times 100 \quad (7)$$

The TNBS assay was also performed on G-CDH to quantify amino groups ($-NH_2$) before and after carbohydrazide modification.[36,40] Gelatin and G-CDH were dissolved in 0.1 M $NaHCO_3$ solution to reach 1 mg mL^{-1} concentration. Then, 0.5 mL of gelatin and G-CDH solutions were added to 0.25 mL of TNBS solution with 0.01% w/v concentration in 0.1 M $NaHCO_3$. After 30 minutes of incubation at 37 °C, the reaction was stopped by adding 0.125 mL of 1 N HCl and then 0.25 mL of 10% w/v sodium dodecyl sulfate (SDS). Finally, the absorbance was read at 335 nm using a microplate reader. The calibration curve was measured with glycine solutions at different concentrations (5–0.008 mM). The degree of modification of gelatin is obtained by eqn (8):

$$\text{Modification degree (mmol g}^{-1}\text{)} = \frac{NH_2 \text{ conc (mM)}}{\text{sample conc (g L}^{-1}\text{)}}$$
$$= \frac{NH_2 \text{ conc (mmol)}}{\text{gelatin (g)}} \quad (8)$$

2.5 PDA pre-hydrogel and PDA/G-CDH hydrogel characterization

2.5.1 Rheological characterization. Rheological analyses were performed using a Modular Compact Rheometer (MCR 302, Anton Paar), equipped with plane discs (upper disc with 15 mm diameter). First, pectin and PDA solutions (4% w/v) were crosslinked with 100 mM $CaCl_2$ in silicon cylindrical molds (10 mm diameter, 1.5 mm height). Then, PDA/G-CDH hydrogels (3% w/v concentration, with 30 mM $CaCO_3$ pre-crosslinking and a PDA/G-CDH ratio of 30 : 70, 50 : 50 and 70 : 30% w/w) were prepared in silicon cylindrical molds and also characterized.

The resulting cylindrical hydrogels were analyzed after a resting time of at least 10 min, with a working gap of 1 mm. Strain sweep analyses were conducted at a constant frequency of 1 Hz, varying strains from 0.01% to 500% to determine the linear viscoelastic (LVE) region. Frequency sweep tests were performed to determine the storage modulus (G') and the loss modulus (G''). They were carried out at a constant strain of 1% (within the LVE region calculated by strain sweep analyses), with frequencies varying from 10 to 0.1 rad s^{-1} and at temperatures of 37 °C.[45] Frequency analysis was used to estimate the Young's modulus (E), according to eqn (9):

$$E = 2\sqrt{G'^2 + G''^2} \cdot (1 + \nu) \quad (9)$$

where ν is the Poisson's ratio (*i.e.* 0.5 for polysaccharide hydrogels) and G' and G'' are the storage modulus and loss modulus at 1 rad s^{-1}, respectively.[45]

Shear rate sweep tests were performed to investigate the non-Newtonian behavior of PDA/G-CDH injectable hydrogels,

varying the shear rate from 0.1 to 500 s^{-1}. The hydrogels' ability to recover their state after injection was estimated by the following three-step oscillation protocol at a constant frequency of 1 Hz and temperature of 37 °C. First, an oscillatory test was carried out for 120 s at 1% strain to assess G', G'' values, then a 500% strain was applied for 60 s to cause a possible structural breakdown, and finally a third oscillatory step was carried out for 100 s at 1% strain to measure the recovery of G', G''. This process was repeated six times.

2.5.2   *In vitro* stability tests. Hydrogel stability was analyzed *versus* time (1, 2, 3, 7, 14 and 21 days) in sterile conditions by incubating 400 μL hydrogel in 2 mL DMEM at 37 °C. The initial weight of each hydrogel sample (W_0) was measured. At each time point, the samples were weighed again (W_i), while DMEM was refreshed. The percentage wet weight variation ($W_\%$) was calculated by eqn (10):

$$W_\% = \frac{W_i}{W_0} \times 100 \qquad (10)$$

2.5.3   Injectability and self-healing. The PDA/G-CDH hydrogel injectability was evaluated on samples prepared in 1 mL Luer-lock syringes, incubated for 30 min and then extruded on microscope slides through different-gauge needles (G20, G21, G22, G25, G27 and G30), while video recording the extrusion at slow motion. Samples were prepared adding food dyes to facilitate the visualization. Injectability was qualitatively classified as follows: (I) the sample can be injected using two hands; (II) the sample can be injected using only one hand; (III) the sample shows a burst release from the needle when injected.[46]

Self-healing behavior of hydrogels was qualitatively assessed by producing hydrogels of different colors on silicon molds. After resting for 30 min, PDA/G-CDH hydrogels were cut in half and re-assembled combining samples with different colors. The strength of the self-healed hydrogels was qualitatively evaluated after 1 and 24 h by handling the samples.[47]

2.5.4   *In vitro* cell viability and adhesion analyses. Human foreskin fibroblasts (HFF-1) were purchased from American Type Culture Collection (ATCC-SCRC-1041) and maintained in DMEM high glucose (Gibco) supplemented with 10% FBS, 1% insulin, and 2% L-glutamine. Cells were maintained at 37 °C in a humidified atmosphere, with 5% CO_2.

In vitro cytocompatibility was evaluated on eluates of PDA pre-hydrogels and PDA/G-CDH hydrogels. All the tested samples were prepared in sterile conditions (as described in the section 2.2.4). HFF-1 were seeded in 96-well plates (6×10^3 cells per well) in complete media for 24 h. Then, culture medium was replaced with conditioned medium, previously obtained by submerging 100 μL of PDA pre-hydrogels and PDA/G-CDH hydrogels in 150 μL complete medium. In control samples, HFF-1 complete medium was used. After 24 h cell culture, the medium was replaced with 100 μL of non-fluorescent resazurin solution composed of CellTiter-Blue® Cell Viability Assay reagent (Promega), diluted 1:10 in new complete medium. Cell viability was evaluated after 3 h incubation in terms of fluorescence intensity, measured by a microplate reader at 560 nm (ex)/590 nm (em) wavelength.

Cell morphology was assessed after 7 days of culture on the selected hydrogels. The hydrogels were prepared under sterile conditions and subsequently placed into 48-well plates. HFF-1 cells were seeded onto the upper surface of the hydrogels at a density of 5×10^4 cells per well and the culture medium was replaced every 2–3 days with an equal volume of fresh medium. After 7 days, the HFF-1 cells were fixed in 4% w/v paraformaldehyde (Alfa Aesar) in PBS for 15 min and subsequently washed with PBS. The cells were permeabilized with Triton X-100 0.5% in PBS for 10 min. Alexa Fluor 488 Phalloidin staining (Life Technologies, USA) was employed for F-actin, while cell nuclei were counterstained with 4′,6-diamidino-2-phenylindole (DAPI). Samples were imaged using the Nikon Ti2-E fluorescence microscope (Nikon Instruments).

2.6   CurZNPs-loaded PDA/G-CDH hydrogel characterization

2.6.1   Release studies of CurZNPs from PDA/G-CDH hydrogels. The release of CurZNPs from PDA/G-CDH hydrogels was evaluated through UV-Vis absorbance and DLS analyses. CurZNPs-loaded PDA/G-CDH hydrogels (100 μL) were placed on the transwells (1 mm mesh size) of 24-well plates, and then incubated with 500 μL of PBS supplemented with $CaCl_2$ (0.1 mg mL^{-1}). The release media were analyzed at 425 nm to detect curcumin. The calibration curve was obtained using CurZNPs suspended in PBS at different concentrations (0.1–100 μg mL^{-1}).

DLS analysis was also carried out on the release media to verify the integrity of CurZNPs during the release studies.

2.6.2   *In vitro* antioxidant and anti-inflammatory potential of CurZNPs-loaded PDA/G-CDH hydrogels. HFF-1 were seeded at a density of 6×10^3 cells per well for 24 h in complete medium. HFF-1 were treated with increasing curcumin concentrations (2.5, 5, 10, 20, 30 or 40 μg mL^{-1}) for 24 h to determine curcumin dose-dependent cytocompatibility. To stimulate oxidative stress, after 7 days' culture, HFF-1 cells were treated with increasing concentrations of H_2O_2 (0.6, 0.8, 1, 1.2 and 1.4 mM) for 3 h.

After setting the parameters, HFF-1 were seeded on 24-well plates (2.2×10^4 cells per well) for 24 h. Then they were pre-treated for 7 days with 100 μL CurZNPs (25 μg mL^{-1})-loaded PDA/G-CDH hydrogels on transwell supports. Subsequently, the pre-treated cells were cultured for 3 h with 800 μM H_2O_2 to stimulate oxidative damage. CellTiter-Blue® Viability Assay was performed to evaluate the antioxidant effect of CurZNPs-loaded PDA/G-CDH hydrogel.[2,48] Untreated cells and cells treated with H_2O_2 alone were used as controls.

Anti-inflammatory evaluations of CurZNPs-loaded PDA/G-CDH hydrogels were performed. CurZNPs-loaded PDA/G-CDH hydrogels were prepared under sterile conditions in silicon cylindrical molds (10 mm diameter, 1.5 mm height) and subsequently placed into 48-well plates. RAW 264.7 cells were seeded onto the upper surface of the hydrogels at a density of 5×10^4 cells per well and the culture medium was replaced every 2–3 days with an equal volume of fresh medium. After 6 days, the cells were treated with LPS (1 μg mL^{-1}) for the last 24 h. Treatment with only LPS was used as a

positive control. After 7 days, the anti-inflammatory activity of CurZNPs-loaded PDA/G-CDH hydrogels was evaluated. NO quantification and CD86 immunostaining were performed as described in the section 2.3.4.

2.7 Statistical analysis

All measurements were made in triplicate unless otherwise stated, and data are presented as mean values ± standard deviation (STD). Statistical analysis of variance (one-way ANOVA) was performed using GraphPad Prism version 9.0.0 for Windows. Tukey's *post-hoc* test was conducted between two or more groups to determine if there were statistically significant differences between populations, in particular, $*p$-value < 0.05, $**p < 0.01$, $***p < 0.001$, and $****p < 0.0001$.

3 Results

This study developed innovative DDSs using injectable pectin-based hydrogels incorporating antioxidant CurZNPs. First, CurZNPs were prepared and characterized in terms of release, antioxidant, and anti-inflammatory properties. Pectin was oxidized and blended with G-CDH to overcome the limitations of native pectin hydrogels, including poor biodegradation, low pH, and limited cell adhesion. Pre-crosslinking PDA with $CaCO_3$ increased the pH to near-physiological levels, while subsequent hydrazone crosslinking between PDA aldehydes and G-CDH amines provided a dual physical–chemical network. PDA/G-CDH hydrogels were optimized across different polymer ratios and characterized for rheology, stability, cytocompatibility, injectability, and self-healing capacity. CurZNPs were then integrated into the hydrogels, achieving hybrid DDS with controlled drug release ability, showing their potential for antioxidant and anti-inflammatory applications.

3.1 Characterization of CurZNPs

Monodisperse CurZNPs (PDI < 0.20) were prepared showing a negative zeta potential and an average hydrodynamic size increasing from 138 nm to 170 nm as the zein to curcumin weight ratio increased, by raising the zein content while maintaining the curcumin at 0.125 mg mL^{-1} (Table 3), in agreement with previous studies.[18,49] Based on their lower size, CurZNPs with an 8:1 weight zein to curcumin ratio were selected for further characterization.

As a comparison, empty zein NPs (ZNPs) showed a mean hydrodynamic diameter of 137 ± 9 nm, a PDI of 0.18 and a negative zeta potential of -21 ± 1 mV. The production yield percentage of empty ZNPs and CurZNPs was approximately 96% and 90%, respectively. CurZNPs exhibited high encapsulation efficiency of around $85 \pm 3\%$.

The release kinetics of curcumin from CurZNPs in physiological (pH 7.4) and acidic (pH 4.8) pH conditions (Fig. 1A) showed a similar trend. An initial 20% burst release was observed after 1 h, increasing to 40% at 3 hours. This was followed by a sustained release profile, with 65% of curcumin released after 1 day, reaching 85% after 2 days and reaching

Table 3 Hydrodynamic diameter, PDI and zeta potential of CurZNPs prepared at different zein to curcumin ratios (with constant 0.125 mg mL^{-1} curcumin concentration), measured by DLS

Zein : curcumin weight ratio (w/w)	CurZNPs		
	Size (nm)	PDI	Zeta potential (mV)
200 : 1	170 ± 3	0.07 ± 0.07	-23 ± 2
50 : 1	187 ± 2	0.15 ± 0.05	-16 ± 1
8 : 1	138 ± 2	0.12 ± 0.01	-17 ± 1

complete release after 7 days. Only a slightly higher amount of curcumin was released at each time point in acidic pH conditions.

The antioxidant activity of CurZNPs was evaluated by the DPPH scavenging assay. CurZNPs showed a high antioxidant activity, with an SC_{50} of 7 µg mL^{-1}, significantly lower than that of free curcumin (13 µg mL^{-1}) and comparable to that of ascorbic acid, the reference antioxidant used as a positive control, which showed an SC_{50} of 5.5 µg mL^{-1} (Fig. 1B). Control empty ZNPs exhibited antioxidant activity at high concentration (SC_{50} of 35 µg mL^{-1}).

Anti-inflammatory evaluation with RAW 264.7 cells showed that high cell viability (84%) was preserved upon treatment with up to 5 µg mL^{-1} CurZNPs while a marked reduction in viability was observed at 10 µg mL^{-1} CurZNPs concentration (46%), as described in Fig. 1C. Based on these results, the 5 µg mL^{-1} dose was confirmed for subsequent experiments. To investigate the anti-inflammatory activity of CurZNPs, RAW 264.7 cells were first polarized to the pro-inflammatory M1 phenotype using LPS. LPS concentrations of 0.05 and 1 µg mL^{-1} were tested to induce inflammation.[50,51] NO production, a marker of M1 macrophage activation, was quantified using the Griess assay to assess the potential dose-dependent effect of LPS on the inflammatory response.[52] As shown in Fig. 1D, NO levels increased fivefold in response to 1 µg mL^{-1} LPS compared with untreated controls and lower LPS dose, indicating successful M1 polarization. This concentration was therefore chosen for further testing.

Based on the above selected parameters, the anti-inflammatory effect of CurZNPs was assessed in LPS-stimulated RAW 264.7 cells. RAW 264.7 cells were cultured for 48 h and then treated with CurZNPs (5 µg mL^{-1} curcumin) and LPS (1 µg mL^{-1}) for 24 h. The ability to induce macrophage polarization by CurZNPs was evaluated by examining the expression of the M1 marker CD86.[53] Immunostaining revealed a significant reduction in CD86 expression in LPS-stimulated cells treated with CurZNPs, both qualitatively (Fig. 1E) and quantitatively by measuring the percentage of CD86-positive cells over total nuclei (Fig. 1F). Specifically, the percentage of CD86-positive cells decreased from 87% in the LPS group to 43% following CurZNPs treatment. Moreover, treatment with CurZNPs significantly reduced NO production to 53% relative to 100% for LPS-only controls (Fig. 1G), demonstrating a strong anti-inflammatory response. Based on these findings, CurZNPs might effectively mitigate inflammatory responses by downregulating
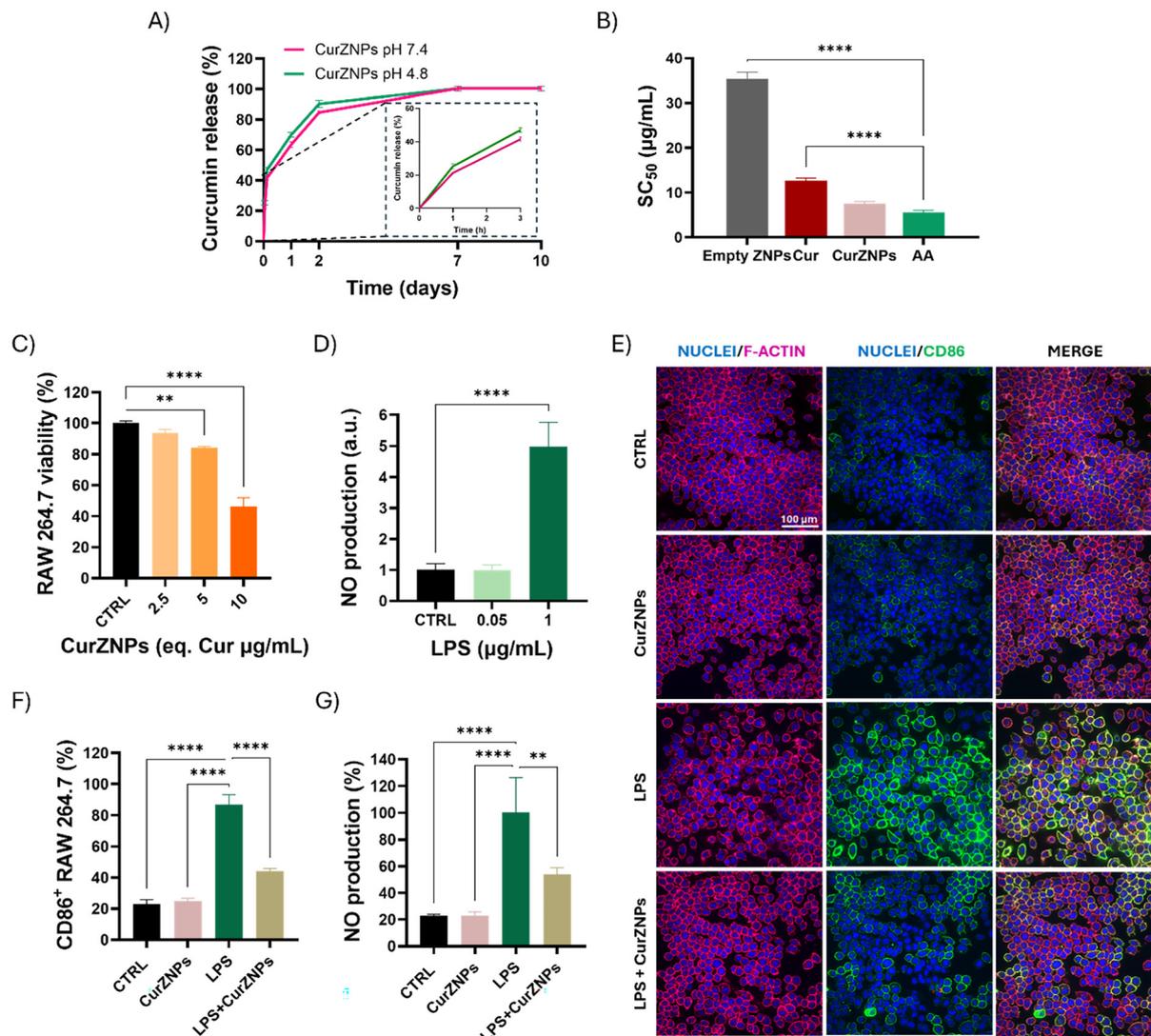
Fig. 1 (A) Curcumin release profile from CurZNPs at 37 °C in PBS, under physiologic (magenta) and acidic (green) pH. (B) DPPH assay results: concentration of empty ZNPs, free curcumin in ethanol (Cur), CurZNPs and ascorbic acid (AA) needed to get 50% DPPH scavenging activity (SC_{50}). (C) RAW 264.7 cell viability after CurZNPs treatment at different curcumin-equivalent concentrations (**$p < 0.01$ and ****$p < 0.0001$, compared to CTRL). (D) RAW 264.7 NO production after LPS stimulation at different concentrations (****$p < 0.0001$, compared to CTRL). (E) RAW 264.7 immunostaining after 24 h CurZNPs and LPS treatments for CD86 (green), with phalloidin staining for F-actin (magenta) and cell nuclei in blue with DAPI (scale bar: 100 μm). (F) Percentage of CD86-positive RAW 264.7 cells over the total nuclei after 24 h of CurZNPs and LPS treatments (****$p < 0.0001$, $n = 12$, compared to LPS). (G) RAW 264.7 NO production after LPS stimulation and CurZNPs treatments (**$p < 0.01$ and ****$p < 0.0001$, $n = 9$, compared to LPS).

M1 macrophage markers and reducing NO production, thus supporting their potential as anti-inflammatory agents.

3.2 PDA synthesis and PDA pre-hydrogel preparation

PDA was synthesized using sodium metaperiodate as oxidation reagent, with two different theoretical oxidation degrees of 2.5% (PDA_2.5) and 5% (PDA_5) and a production yield of 76 ± 11% and 83 ± 8%, respectively. The real oxidation degree values, measured by the TNBS assay, were 2.3 ± 0.4% for PDA_2.5 and 4.5 ± 0.8% for PDA_5 (Fig. 2A).

ATR-FTIR analysis of pectin and PDA (Fig. 2B) confirmed successful oxidation. In the ATR-FTIR spectra of PDA the

absorbance band at 1740 cm^{-1}, attributed to the stretching vibration of ester carbonyl groups, became narrower and slightly shifted towards lower wavenumbers (1734 cm^{-1}) with respect to the pectin spectrum due to the introduction of C=O from aldehyde groups, thus confirming pectin successful oxidation.[32] Additionally, the absorption band at 1614 cm^{-1}, corresponding to the symmetric vibrational stretching of free carboxylate COO$^-$ groups, showed increased intensity, with respect to the C=O stretching band, as a function of the oxidation degree. This phenomenon has been attributed to the partial ionization of carboxylic acid (–COOH) groups on the polysaccharide backbone, which occurs above a threshold pH
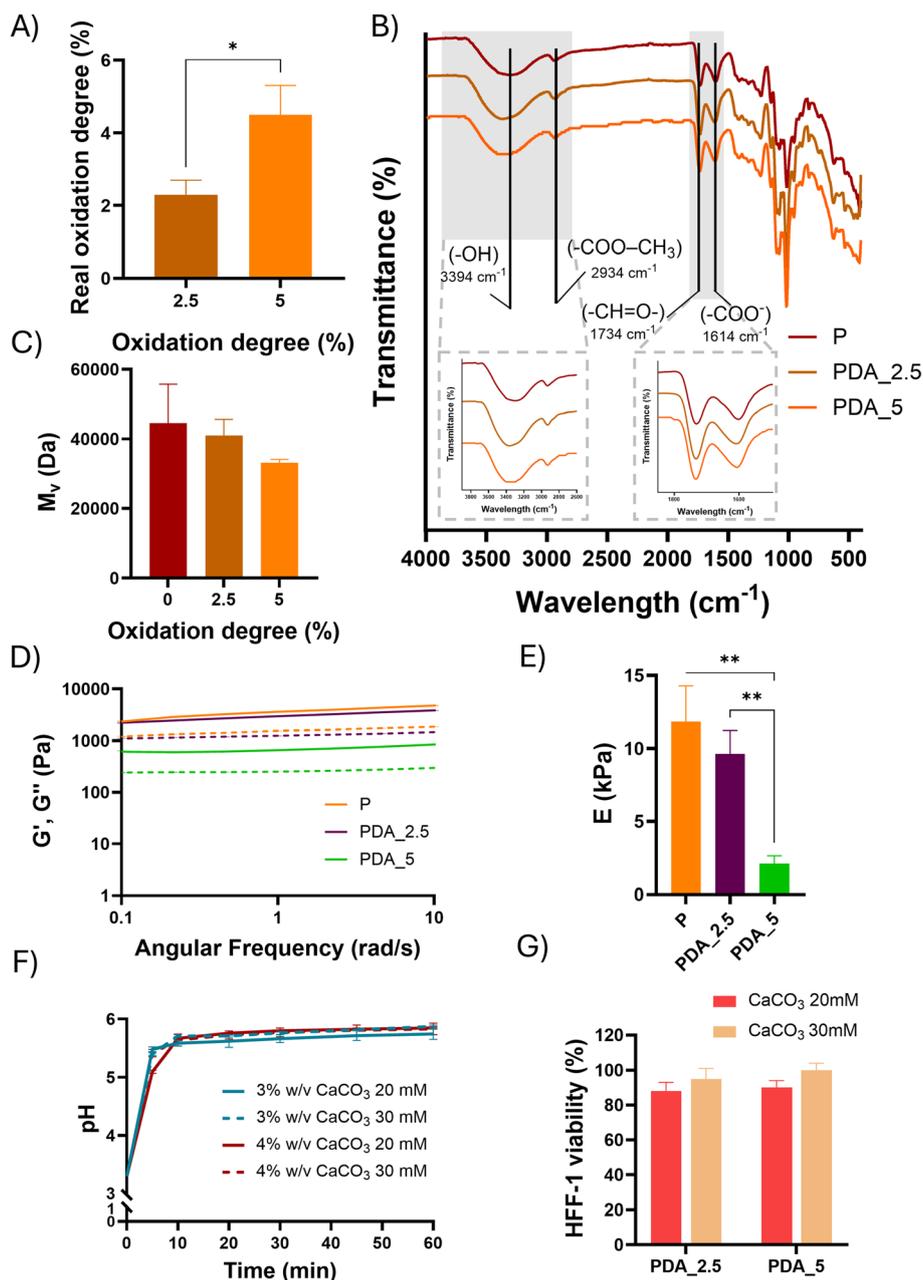
Fig. 2 (A) Aldehydic content of PDAs (%mol of aldehyde/mol of galacturonic acid). (B) ATR-FTIR spectra of pectin (*P*), PDA_2.5 and PDA_5 (*$p <$ 0.05). (C) Viscosimetric molecular weight of pectin, PDA_2.5 and PDA_5, as a function of the theoretical oxidation degree. (D) Storage modulus (G', continuous line) and loss modulus (G'', dotted line) of pectin (orange), PDA_2.5 (purple) and PDA_5 (green) at 4% w/v total polymer concentration, crosslinked with 100 mM CaCl$_2$ as a function of angular frequency (1–10 rad s^{-1}) at 37 °C. (E) Elastic modulus (E) derived from frequency sweep tests (1 rad s^{-1}) of pectin (orange), PDA_2.5 (purple) and PDA_5 (green) at 3% w/v total polymer concentration (**$p <$ 0.01). (F) pH of PDA_2.5 and PDA_5 hydrogels (3 and 4% w/v) treated with 20 or 30 mM CaCO$_3$ as a function of time. (G) Indirect cell viability tests of HFF-1 cells treated with eluates from 3% w/v PDA_2.5 and PDA_5 hydrogels crosslinked with either 20 or 30 mM CaCO$_3$. Control HFF-1 cells were cultured on tissue culture plastic plates using untreated media.

of approximately 2.5.[32] The absorbance band due to COO–CH$_3$ methyl stretching vibrations in galacturonic acid slightly shifted from 2934 cm^{-1} to 2925 cm^{-1} as a function of the oxidation degree.[39] Furthermore, the OH stretching band at 3338 cm^{-1} weakened and shifted to 3394 cm^{-1}, corresponding to a reduction in the number of hydroxyl groups following oxi-

dation. This spectral change confirms the selective oxidation of pectin α-diols, resulting in the formation of two aldehyde groups per oxidized monomeric unit.[44,54]

The viscosimetric molecular weight (M_v) of PDAs was measured using an Ubbelohde viscometer through the Houwink–Sakurada equation (eqn (6)). A decreasing trend of

the viscosimetric molecular weight was detected with increasing the PDA oxidation degree: M_v was 45 ± 11 kDa for unmodified pectin (P), 41 ± 4.6 kDa for PDA_2.5 and 33 ± 9 kDa for PDA_5 (Fig. 2C).

Rheological analysis of pectin and PDA solutions (4% w/v) treated with calcium ions (from CaCl$_2$ 100 mM for 10 min)[44] was performed to assess their ionic crosslinking ability by assessing the formation of stable gels ($G' > G''$) and rheological properties as a function of the oxidation degree. PDA_2.5 and PDA_5 hydrogels retained their crosslinking ability, as demonstrated by G' higher than G'' values in the frequency sweep tests, confirming the formation of stable hydrogel networks (Fig. 2D). Storage modulus values of hydrogels at 1 rad s^{-1} decreased as a function of oxidation degree, taking values of 3620 ± 69 Pa, 2956 ± 16 Pa and 657 ± 5 Pa for pectin, PDA_2.5 and PDA_5 hydrogels, respectively (Fig. 2D). Therefore, Young's modulus of unmodified pectin and PDA_2.5 hydrogels exhibited significant higher values (11.8 ± 2.5 kPa and 9.7 ± 1.6 kPa, respectively) compared to 2.1 ± 0.5 kPa for PDA_5 (Fig. 2E).

To increase the pH of PDA_2.5 and PDA_5 pre-hydrogels (3 and 4% w/v), as explained in the experimental part, PDA solutions in 20 mM NaHCO$_3$ (pH ∼3.3) had CaCO$_3$ (20 and 30 mM in PBS) added to them.[31] Pre-hydrogels at 3% w/v polymer and with 30 mM CaCO$_3$ reached a near-physiological pH more rapidly than the other tested conditions, with a pH of 5.6 within 5 min and increasing to 5.9 after 30 min (Fig. 2F). In contrast, other formulations showed a slower pH adjustment, ranging from 5.0–5.4 at 5 min and rising to 5.8 after 30 min. Based on their faster pH recovery, which promotes more efficient pre-hydrogel formation, formulations with 3% w/v polymer content and 30 mM CaCO$_3$ were selected for further evaluation.

PDA_2.5 and PDA_5 pre-hydrogels with 3% w/v concentration and either 20 and 30 mM CaCO$_3$ were assessed for potential CaCO$_3$-induced cytotoxicity in vitro using HFF-1 cells. Both tested conditions demonstrated good cytocompatibility. Since PDA hydrogels crosslinked with 30 mM CaCO$_3$ showed a slightly higher cytocompatibility (Fig. 2G), they were confirmed for further use.

3.3 PDA/G-CDH hydrogels

G-CDH was prepared by carbodiimide-mediated grafting of carbohydrazide functionalities[36,55] with a 37 ± 2.4% modification degree (Fig. 3A) and a yield of 92 ± 4%. Then, PDA_2.5/G-CDH and PDA_5/G-CDH hydrogels (3% w/v, 30 mM CaCO$_3$) were prepared at three PDA : G-CDH ratios (30 : 70, 50 : 50 and 70 : 30% w/w). Rheological analysis showed the tunable mechanical properties of PDA/G-CDH hydrogels as a function of PDA oxidation degree and PDA to G-CDH ratio (Fig. 3B and C). PDA_5/G-CDH hydrogels exhibited higher G' values than PDA_2.5/G-CDH hydrogels. Among the tested PDA_2.5/G-CDH hydrogels, PDA_2.5/G-CDH 70 : 30 composition showed the highest G' value at 1 rad s^{-1} (45 ± 2 Pa). On the other hand, for the PDA_5/G-CDH hydrogels, the PDA_5/G-CDH 50 : 50 composition showed the highest G' value (115 ± 20 Pa). Young's modulus measurements showed elastic moduli in the range of hundreds of Pascals (132 ± 5 for PDA_2.5/G-CDH hydrogels

and 342 ± 61 Pa for PDA_5/G-CDH hydrogels) (Fig. 3D). For the two hydrogel types, these compositions corresponded to an aldehyde to amino groups ratio of 0.86 and 1.22, respectively, as determined through TNBS analysis (Fig. 3E).

In vitro stability tests of PDA/G-CDH hydrogels, performed at 37° C under sterile conditions in DMEM for 21 days, showed a decrease in the wet weight over time (Fig. 3F). Hydrogels with the lowest PDA content showed the highest weight loss of approximately 50%. Conversely, PDA_2.5/G-CDH (70 : 30) hydrogels exhibited the highest stability over time. After 21 days of incubation, PDA_2.5/G-CDH (70 : 30) and PDA_5/G-CDH (50 : 50) hydrogels showed 26% and 38% weight loss, respectively. Due to their enhanced stability, PDA_2.5/G-CDH (70 : 30) and PDA_5/G-CDH (50 : 50) hydrogels were chosen for further characterization.

Hydrogel injectability was qualitatively evaluated by testing hydrogel extrusion through syringes with different needle sizes (Fig. 4A and B). Three levels of injectability were assessed after hydrogel complete gelation (i.e., >30 min incubation): injectability by pressing the syringe plunger with (I) both hands and (II) one hand only; and (III) the evidence of a burst release from the needle (hydrogels requiring high injection force can technically be injected, but excessive pressure may damage local tissues and reduce retention by rupturing nearby blood vessels).[46] For each injectability level, a green, yellow or red box was used to indicate successful completion of the injectability tests, or the obtainment of intermediate or unsatisfactory results, respectively. Both hydrogel types could be easily injected through needles with decreasing size up to 27-G. Hydrogel injectability was further studied by rheological analysis. Shear sweep tests were conducted to evaluate the viscosity of PDA/G-CDH hydrogels versus shear rate. As depicted in Fig. 4C, both PDA_2.5/G-CDH (70 : 30) and PDA_5/G-CDH (50 : 50) hydrogels exhibited a shear-thinning behavior.

A three-step rheological test was exploited to investigate the self-healing behavior of PDA_2.5/G-CDH (70 : 30) and PDA_5/G-CDH (50 : 50) hydrogels (Fig. 4D). Both samples exhibited rapid sol-to-gel and gel-to-sol transition upon changes in strain. Qualitative assessment of self-healing behavior of PDA_2.5/G-CDH (70 : 30) and PDA_5/G-CDH (50 : 50) hydrogels with both rectangular and circular shapes was performed by placing two cut samples of the same, loaded with a blue and a yellow dye, in direct contact (Fig. 4E and F). After 1 h, an intermediate color formed at the interface between the two samples, suggesting dye interdiffusion. After 24 h, the intermediate color extended almost to a larger portion of the samples (Fig. 4E). At each time-point, the assembled samples were also handled with scoops and tweezers to qualitatively investigate their response to tensile and torsional stresses. PDA_2.5/G-CDH (70 : 30) hydrogels showed superior resistance to twisting and stretching; on the other hand, PDA_5/G-CDH (50 : 50) samples were less mechanically resistant (Fig. 4F).

Finally, in vitro cytocompatibility and cell adhesion tests were performed on PDA_2.5/G-CDH (70 : 30) and PDA_5/G-CDH (50 : 50) using HFF-1 cells. Both hydrogels exhibited an average cell viability close to 100% up to 7 days culture time,
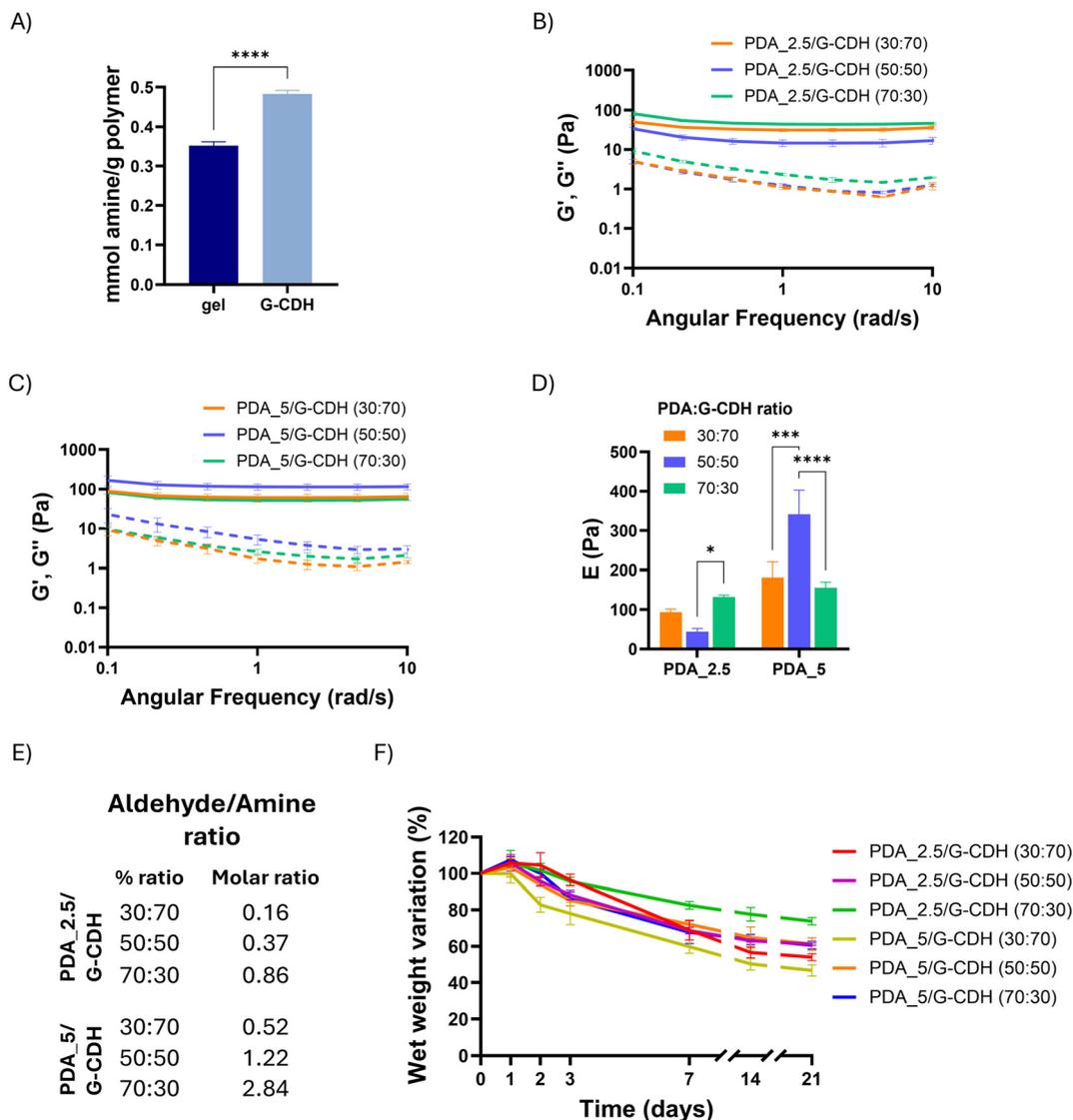
Fig. 3 (A) Primary amino group content of gelatin and G-CDH (m of amines/g of polymer) (****$p < 0.0001$). (B) PDA_2.5/G-CDH and (C) PDA_5/G-CDH storage modulus (*G'*, continuous line) and loss modulus (*G''*, dotted line) as a function of angular frequency (1 and 10 rad s^{-1}) at 37 °C at different PDA : G-CDH ratios, *i.e.*, 30 : 70 (orange), 50 : 50 (blue) and 70 : 30 (green). (D) Elastic modulus (*E*) derived from frequency sweep tests of PDA_2.5/G-CDH and PDA_5/G-CDH hydrogels at 1 rad s^{-1} (*$p < 0.05$, ***$p < 0.001$ and ****$p < 0.0001$). (E) Aldehyde (of PDA_2.5 and PDA_5) to amine (of G-CDH) ratio according to TNBS data for 30 : 70, 50 : 50 and 70 : 30% w/w ratios. (F) Wet weight loss percentage of PDA_2.5/G-CDH and PDA_5/G-CDH hydrogels incubated in PBS ($n = 4$).

with no significant differences among samples (Fig. 5A). Furthermore, both hydrogels supported cell adhesion and spreading, as demonstrated by complete cell coverage of the hydrogel surface (Fig. 5B).

3.4 Characterization of CurZNPs-loaded hydrogels

Hydrogels loaded with free curcumin (Cur) showed a more gradual and sustained curcumin release than free CurZNPs (Fig. 6A). On the other hand, PDA_2.5/G-CDH (70 : 30) and PDA_5/G-CDH (50 : 50) hydrogels loaded with CurZNPs showed a more controlled and sustained curcumin release compared to hydrogels containing Cur. Indeed, after 3 days, the average curcumin release from CurZNPs-loaded PDA_2.5/G-CDH

(70 : 30) and PDA_5/G-CDH (50 : 50) hydrogels was 40 and 33%, *versus* 77 and 85% for Cur-loaded PDA_2.5/G-CDH (70 : 30) and PDA_5/G-CDH (50 : 50) hydrogels, respectively. Complete release for Cur-loaded hydrogels was achieved after approximately only 7 days, but after 28 days for CurZNPs-loaded hydrogels. Since CurZNPs-loaded PDA_2.5/G-CDH (70 : 30) showed a more sustained curcumin release over 21 days, this composition was chosen for further *in vitro* cell tests. Moreover, DLS analysis of release media was performed at each time point to evaluate CurZNPs release (Table S1). Fig. S3 reports CurZNPs size measurements by DLS analysis at some illustrative time points of CurZNPs release (1, 3 and 7 days) from both hydrogels.
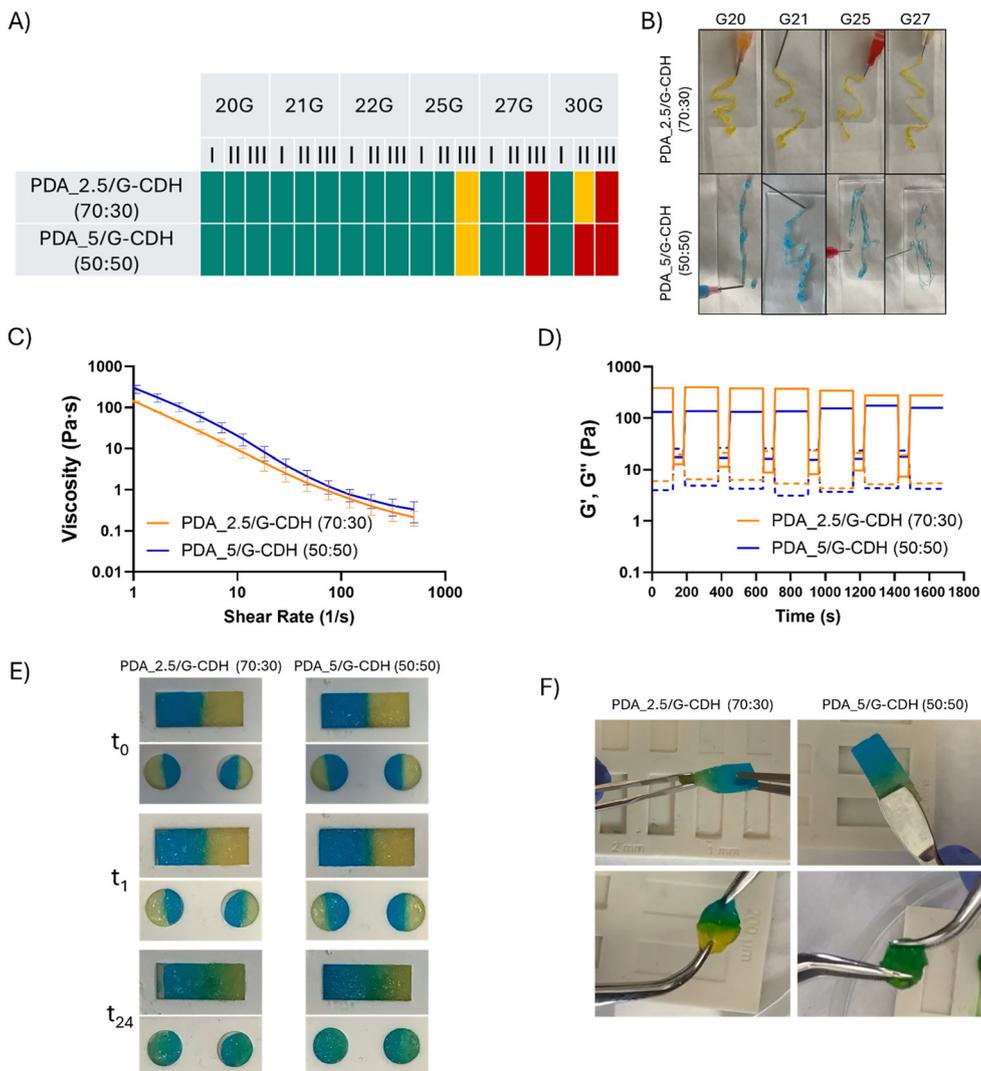
Fig. 4 (A and B) Qualitative assessment of hydrogel injectability: after 30 min crosslinking, PDA_2.5/G-CDH (70 : 30) and PDA_5/G-CDH (50 : 50) hydrogels were manually extruded using syringes with 20–30 Gauge (G) needles. (C) Viscosity curve as a function of the shear rate for PDA_2.5/G-CDH (70 : 30) (orange) and PDA_5/G-CDH (50 : 50) (blue) hydrogels. (D) Recovery curve of PDA_2.5/G-CDH (70 : 30) (orange) and PDA_5/G-CDH (50 : 50) (blue) hydrogels. (E) Self-healing evaluation: two previously cut parts of PDA_2.5/G-CDH (70 : 30) (left) and PDA_5/G-CDH (50 : 50) (right) hydrogels, loaded with a blue and a yellow dye, were put into direct contact, and healing was studied at different times (0 h, 1 h and 24 h). Dye inter-diffusion at the contact interface was evidenced by the formation of an intermediate green color. (F) Qualitative assessment of the effects of bending and stretching stresses on the self-healed PDA2.5/G-CDH (70 : 30) and PDA_5/G-CDH (50 : 50) hydrogels.

To better understand the curcumin release mechanism from CurZNPs, free curcumin (Cur)-loaded PDA/G-CDH hydrogels and CurZNPs-loaded PDA/G-CDH hydrogels, the experimental cumulative release data were fitted using the Ritger–Peppas model:[56,57]

$$\frac{M_t}{M_\infty} = kt^n \tag{11}$$

where M_t is the amount of drug released at time t, M_∞ is the total amount of released drug, k is a kinetic constant, and n is the diffusional exponent. Results are reported in Table 4.

The fitting showed high correlation coefficients (R^2 ranging from 0.92 to 0.99), confirming that the chosen model is a good fit for our experimental data. CurZNPs alone exhibited a release exponent n of 0.25. This low value is associated with a rapid burst release, dominated by Fickian diffusion (identified for $n < 0.5$), typical of NPs. Hydrogels loaded with free curcumin showed significantly higher n values ($n = 0.83$ and 0.84), indicating the so-called Case II transport (for $0.5 < n < 1$), where curcumin release is governed by a combination of Fickian diffusion and polymer network relaxation. Notably, CurZNPs-loaded hydrogels also displayed n values within the Case II transport regime ($n = 0.84$–0.87), but with markedly lower kinetic constants ($k = 0.11$–0.13) compared to free-curcumin-loaded hydrogels ($k = 0.20$). This reflects a slower release rate and demonstrates the additional diffusion resistance
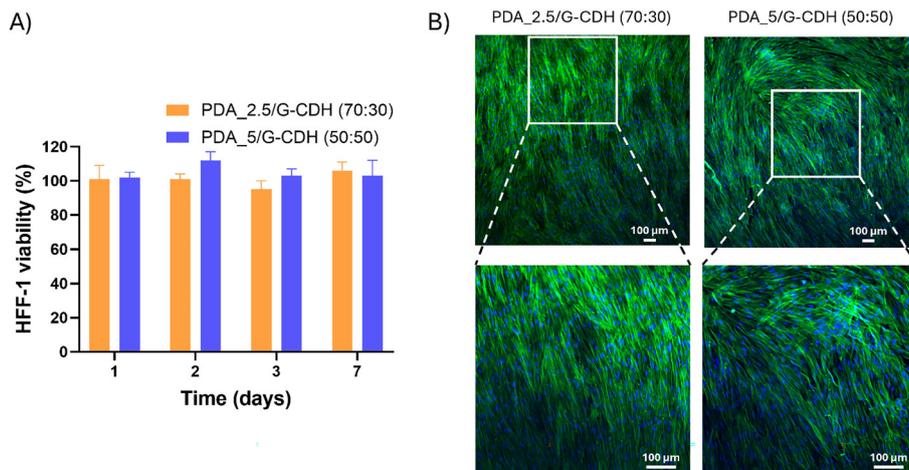
Fig. 5 (A) Indirect cell viability studies of HFF-1 cells, treated with eluates from 3% w/v PDA_2.5/G-CDH (70 : 30) (orange) and PDA_5/G-CDH (50 : 50) (blue) hydrogels, and cultured for 1–7 days. Control samples are HFF-1 cells cultured on tissue culture plastic with untreated media. (B) Phalloidin staining for F-actin (green) and DAPI staining for cell nuclei (blue) of HFF-1 cells directly cultured on the surface of PDA_2.5/G-CDH (70 : 30) (orange) and PDA_5/G-CDH (50 : 50) hydrogels for 7 days. Magnified portions of both images are reported at the bottom.

introduced by encapsulation of curcumin within ZNPs embedded in the hydrogel network.

Then the effect of oxidative stress induced by the H_2O_2 treatment of cultured HFF-1 cells was evaluated. After 7 days' culture, HFF-1 cells were treated with H_2O_2 for 3 h, showing a H_2O_2 dose-dependent decrease of cell viability, reaching 63 ± 5 and 44 ± 6% viability at 0.8 and 1 mM H_2O_2 concentrations, respectively (Fig. 6B).

Then, the dose-dependent effect of 24 h curcumin treatment on HFF-1 cells was evaluated. Cell viability was not affected by increased doses of curcumin up to 5 μg mL^{-1} (Fig. 6C), while a significant decrease of cell viability was observed at higher (10, 20 and 40 μg mL^{-1}) curcumin concentrations. Therefore, 5 μg mL^{-1} curcumin equivalent concentration was selected for CurZNPs-embedded PDA_2.5/G-CDH (70 : 30) hydrogels. HFF-1 pretreatment with CurZNPs-loaded PDA_2.5/G-CDH (70 : 30) hydrogels was able to protect cells against H_2O_2-induced damage (using 0.8 mM H_2O_2-concentration). Fig. 6D shows that while H_2O_2 treatment of HFF-1 cells caused a significant decrease in cell viability (~60%), cell pretreatment with CurZNPs-loaded PDA_2.5/G-CDH significantly restored high viability (~98%). On the other hand, Cur-loaded PDA_2.5/G-CDH (70 : 30) hydrogels exhibited a slight enhancement in cell viability after exposure to H_2O_2-induced stress (~83%), while Cur and CurZNPs were not able to protect cells from oxidative stresses.

Finally, the anti-inflammatory activity of the CurZNPs-loaded PDA_2.5/G-CDH (70 : 30) was evaluated *in vitro* using macrophages to investigate the efficacy of the released CurZNPs. This study aimed to determine whether their sustained release from the PDA_2.5/G-CDH (70 : 30) hydrogel matrix could extend the anti-inflammatory response for a prolonged period. After 7 days, CurZNPs-loaded hydrogels produced a pronounced reduction in NO levels in LPS-stimulated

cells, decreasing NO production to 7% compared to the controls, whereas free CurZNPs reduced it only to 62% (Fig. 7A). Immunofluorescence staining further supported these findings, since LPS stimulation led to strong CD86 expression while cells treated with hydrogel-releasing CurZNPs showed a visibly attenuated CD86 signal (Fig. 7B). In contrast, free CurZNPs induced only a partial decrease in CD86 expression. Overall, macrophages exposed to CurZNPs released from the hydrogel displayed lower inflammatory marker levels, suggesting the greater anti-inflammatory efficacy achieved through sustained release from the hydrogel matrix.

4. Discussion

Oxidative stress and inflammation are tightly intertwined biological processes that play a central role in the pathogenesis and progression of numerous chronic and acute diseases, involving the coordinated interaction of cells, tissues and growth factors to restore tissue integrity. However, the healing process can be impaired largely due to oxidative stress caused by the excessive accumulation of ROS.[1,9] To counteract the detrimental effects of oxidative stress, antioxidant therapies have emerged as promising therapeutic strategies to scavenge ROS and promote a more favorable healing environment. Several antioxidants have been studied for their ability to improve soft tissue healing by reducing inflammation, enhancing collagen synthesis and protecting cells from oxidative damage. Among them, curcumin has demonstrated strong antioxidant properties, thanks to its ability to scavenge free radicals and to reduce pro-inflammatory cytokine production, resulting in an effective agent for improving the healing outcomes.[8,58] However, one main challenge of antioxidant therapies is the design of efficient systems for controlled and sustained drug
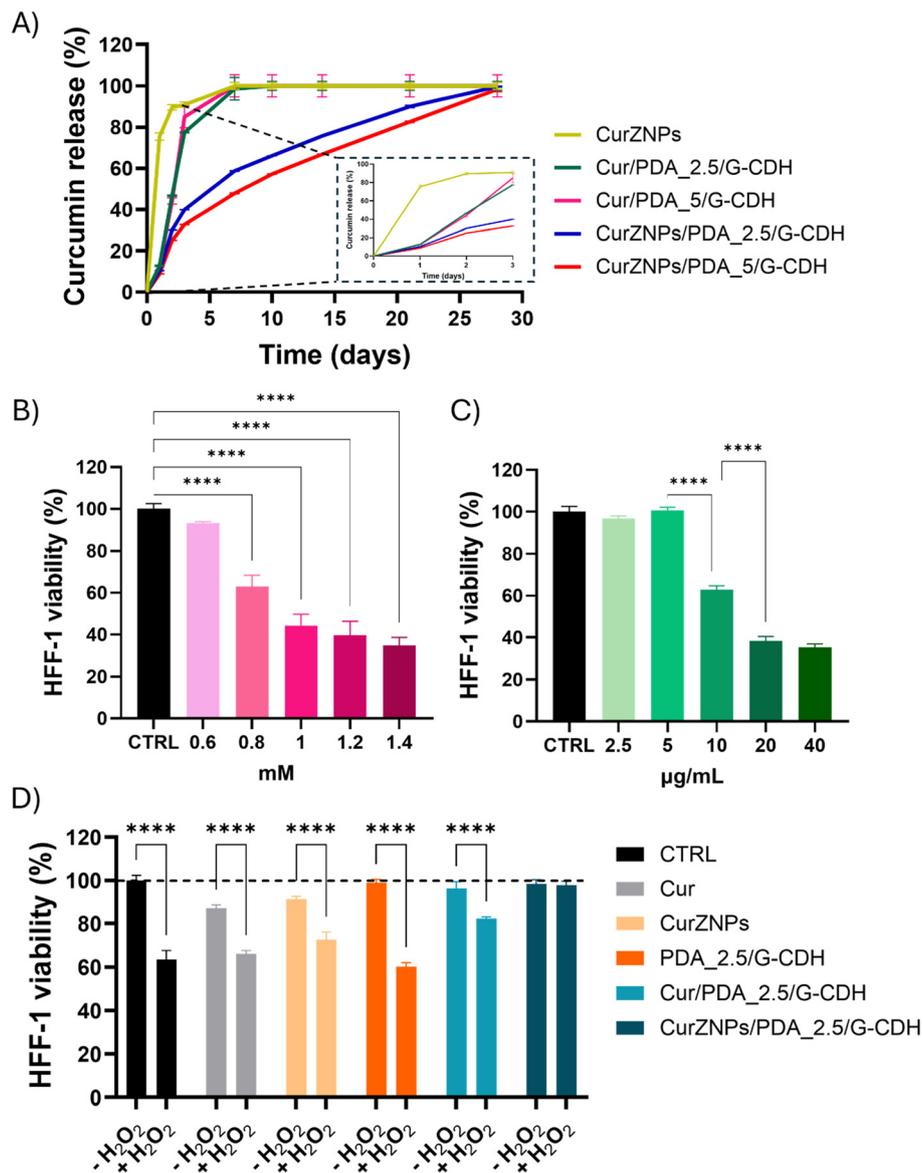
Fig. 6 (A) *In vitro* curcumin percentage release from free curcumin (Cur) and CurZNPs-loaded PDA_2.5/G-CDH (70 : 30) and PDA_5/G-CDH (50 : 50) hydrogels at 37 °C in PBS supplemented with $CaCl_2$ (0.1 mg mL^{-1}). (B) Viability of HFF-1 cells, previously cultured for 7 days, upon further 3 h treatment with different concentrations of H_2O_2 (0.6, 0.8, 1, 1.2 and 1.4 mM). (C) HFF-1 cell viability after curcumin treatments at different concentrations (2.5, 5, 10, 20, 40 μg mL^{-1}) for 24 h. (D) HFF-1 cell viability after 7-days' treatment with free curcumin (Cur)- and CurZNPs-loaded PDA_2.5/G-CDH (70 : 30) hydrogel, followed by 0.8 mM H_2O_2 treatment for 3 h.

Table 4 Ritger–Peppas model outputs for curcumin release modeling from CurZNPs, free curcumin (Cur) and CurZNPs-loaded PDA_2.5/G-CDH (70 : 30) and PDA_5/G-CDH (50 : 50) hydrogels at 37 °C in PBS supplemented with $CaCl_2$ (0.1 mg mL^{-1})

	n	k	R^2
CurZNPs	0.25	0.76	0.99
Cur/PDA2.5/G-CDH	0.83	0.20	0.94
Cur/PDA5/G-CDH	0.84	0.20	0.92
CurZNPs/PDA2.5/G-CDH	0.87	0.13	0.98
CurZNPs/PDA5/G-CDH	0.84	0.11	0.97

delivery to the target site, to address the poor bioavailability and rapid biodegradability of released agents. Curcumin-loaded NPs offer an innovative approach to overcome issues in drug delivery. Indeed NPs may protect curcumin from rapid degradation and enable its sustained release, ensuring antioxidant activity over an extended time period. This results in an enhancement of efficacy treatment, minimizing the need for frequent reapplications, improving patient compliance and outcomes.[16,43,49] In this study, sustainable biodegradable biomaterials, such as pectin and zein, were exploited to design novel injectable DDS hydrogels able to deliver antioxidant-loaded NPs, thereby combining innovation and sustainability.[14,59]
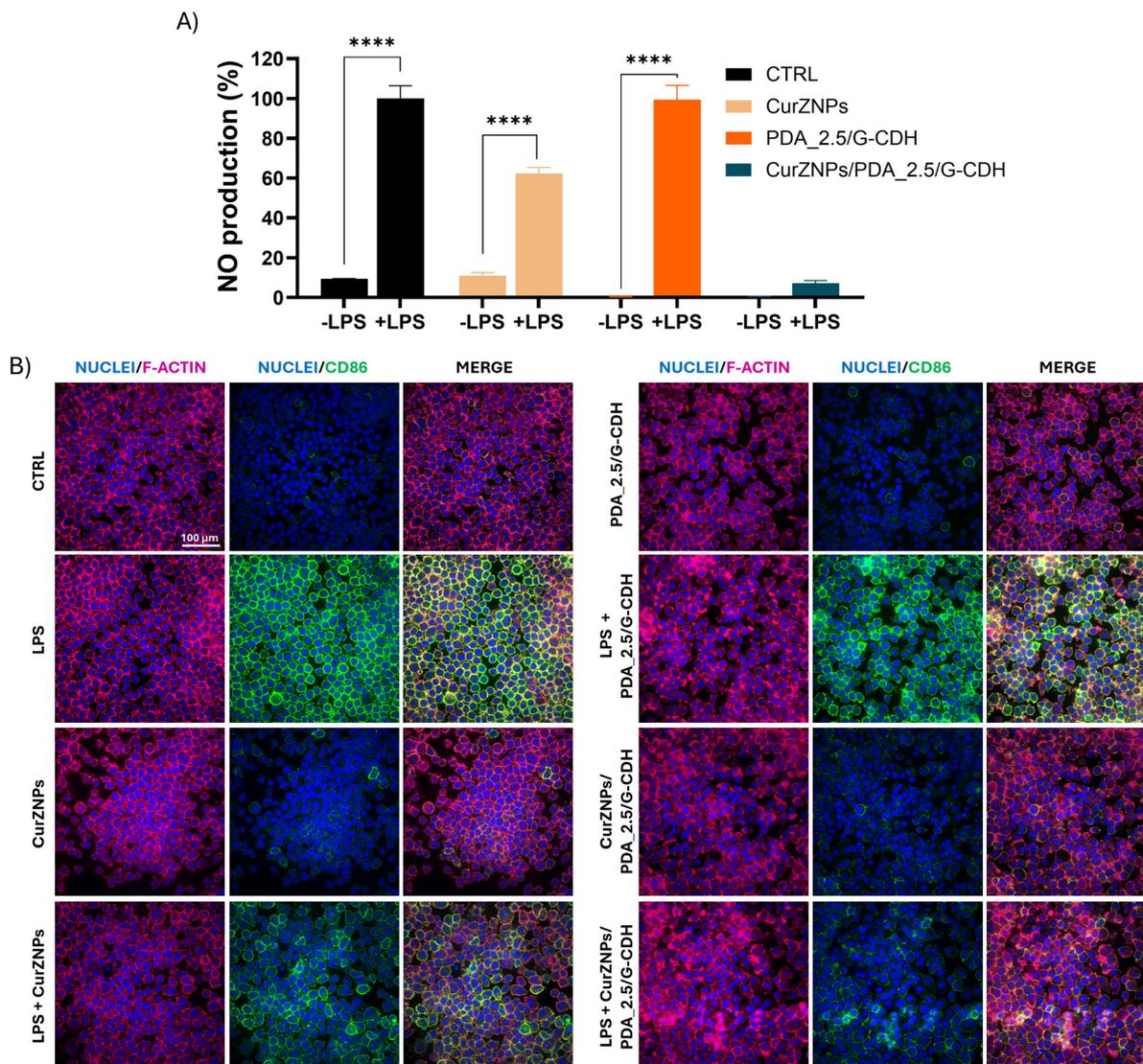
Fig. 7 (A) NO production after 24 h LPS stimulation of RAW 264.7 cells cultured directly on the surface of CurZNPs loaded into PDA_2.5/G-CDH (70 : 30) hydrogel for 7 days (****$p < 0.0001$, $n = 6$, LPS-treated conditions relative to each corresponding condition without LPS). (B) RAW 264.7 immunostaining after 24 h LPS stimulation of RAW 264.7 cells cultured directly on the surface of CurZNPs loaded into PDA_2.5/G-CDH (70 : 30) hydrogel for 7 days for CD86 (green), with phalloidin staining for F-actin (magenta) and cell nuclei in blue with DAPI (scale bar: 100 μm).

Zein was selected as a biocompatible and biodegradable polymer from sustainable sources for NPs loading curcumin. CurZNPs were produced *via* nanoprecipitation minimizing zein concentration (1 mg mL^{-1}), compared to previous studies making use of high zein concentrations (>5 mg mL^{-1} and often around 20–25 mg mL^{-1}). A reduction in zein amount minimizes the ZNPs' risk of triggering an immune response and protein aggregation.[16] Additionally, it leads to the formation of ZNPs with lower sizes that are expected to improve drug release kinetics by enabling a controlled and sustained release of curcumin.[16] Hence, reducing the zein to curcumin weight ratio from 200 : 1 to 8 : 1 w/w ratio decreased the CurZNPs' hydrodynamic diameter from 170 nm to 138 nm, respectively (Table 3). CurZNPs with the smaller size were selected for further studies. This formulation was stable in

aqueous solutions at pH~6–7 (Table 3),[18,49] showing a narrow size distribution (PDI < 0.20) and negative zeta potential value (due to zein's inherent negative charge).[18,49] No significant structural impact in terms of size and zeta potential from curcumin addiction in CurZNPs was detected compared to empty zein NPs (ZNPs), beyond a slight increase in PDI, likely due to the reduced hydrophobic interactions between the zein and curcumin.

The high percentage yields of both ZNPs (96%) and CurZNPs (90%) highlight the efficiency of the preparation method. Moreover, CurZNPs exhibited high encapsulation efficiency (~85%) compared to previous studies, underlining the improved design of this system.[16,43] The kinetic release profiles of curcumin from CurZNPs revealed a two-phase mechanism: an initial burst (20% within 1 hour), followed by

a sustained release, with curcumin release being more gradual in acidic conditions (Fig. 1A). The complete release of curcumin within 7 days underscores the potential of CurZNPs in applications where sustained therapeutic action is critical. Indeed, ZNPs offer high resistance to degradation by proteolytic enzymes, ensuring their release stability also in harsh pH conditions and supporting their use as robust nanocarriers in various clinical settings.[60] CurZNPs demonstrated strong antioxidant activity in the DPPH assay, where a lower SC_{50} value indicates higher free radical scavenging capacity. Compared to Cur, CurZNPs exhibited enhanced free radical scavenging capacity, close to the value for ascorbic acid, a well-known strong antioxidant used as positive control (Fig. 1B). Interestingly, empty ZNPs exhibited intrinsic antioxidant activity at high concentrations, probably due to zein xanthophyll pigment content (8%–9%).[14] This synergistic effect, combined with the therapeutic action of curcumin, might add significant value for antioxidant and anti-inflammatory applications.

The anti-inflammatory potential of CurZNPs was investigated using RAW 264.7 macrophages, as they play a central role in orchestrating immune responses and are primary mediators of inflammation, making them a relevant model for assessing CurZNPs' immunomodulatory effects. CurZNPs maintained high cell viability up to 5 μg mL^{-1} curcumin-equivalent concentration, while cytotoxic effects were observed at the higher dose (Fig. 1C). Based on these results, 5 μg mL^{-1} dose was selected for subsequent anti-inflammatory studies. Macrophages exhibit remarkable plasticity when exposed to various microenvironmental stimuli, predominantly polarizing into two distinct phenotypes: the pro-inflammatory M1-type and the anti-inflammatory M2-type, which perform nearly opposite functions.[53] In response to LPS, M0 macrophages polarize into the M1 phenotype, triggering an inflammatory response through the release of pro-inflammatory molecules. Conversely, exposure to IL-4 and IL-13 induces a shift towards the M2 phenotype, promoting anti-inflammatory activity, tissue repair, and tissue healing by secreting anti-inflammatory molecules. In pathological conditions, M1 macrophages may be unable to fully transition to the M2 phenotype, impairing regeneration, and exacerbating inflammation. Therefore, to mimic an inflammatory environment, RAW 264.7 were polarized to the pro-inflammatory M1 phenotype by LPS treatment. The pro-inflammatory response of RAW 264.7 cells to LPS stimulation was assessed by spectrophotometrically measuring nitrites, the degradation products of NO. NO is a key molecule in inflammation regulation, released by activated macrophages in response to stimuli like pathogens, and is widely used as an *in vitro* inflammation marker.[52] Among the two tested concentrations, 1 μg mL^{-1} LPS induced a robust inflammatory response, as evidenced by a fivefold increase in NO production (Fig. 1D).[51] CurZNPs treatment of LPS-stimulated RAW 264.7 significantly reduced the NO levels to 53% compared to the LPS-only control (100%), indicating a strong anti-inflammatory effect (Fig. 1G). Furthermore, previous literature has shown that curcumin was also found to drive

macrophage polarization by decreasing the M1 phenotype marker CD86.[61] Immunostaining images showed that CurZNPs effectively reduced CD86 expression, lowering the percentage of CD86-positive cells from 87% of LPS-only to 43% of CurZNPs-treated (Fig. 1E and F). Together, these results suggest that CurZNPs effectively attenuate macrophage inflammation by suppressing NO production and downregulating the M1 polarization marker CD86.

With their high water content and ECM-mimicking three-dimensional structure, hydrogels serve as an effective platform for site-specific therapeutic delivery, particularly in the form of injectable systems that enable a precise localization and prolonged treatment of deep lesions.[55] Pectin was selected for hydrogel preparation due to its natural abundance, sustainability, and versatility as an anionic polysaccharide derived from fruit peels, addressing agricultural waste while offering biocompatibility and cost-effectiveness. To overcome its poor *in vivo* biodegradability, pectin was oxidized into pectin dialdehyde (PDA) using sodium metaperiodate.[44,54] Oxidation introduces aldehyde groups while reducing the molecular weight of the polymer. A balance in PDA functionalization and structural integrity is needed, as a high oxidation degree results in an excessively low molecular weight, limiting applications.[32,40] State of the art literature has shown that a 1% oxidation degree results in a 20% reduction in molecular weight, increasing to 57% for medium oxidation levels (∼34%). Since previous studies primarily focused on medium oxidation levels, also 10 and 25% (*i.e.*, PDA_10 and PDA_25) degrees of oxidation were investigated (SI). However, due to excessive chemical modification and reduced molecular weight, PDA_10 and PDA_25 failed to form stable hydrogels through calcium ion-mediated crosslinking. Based on this evidence, two oxidation levels (*i.e.*, 2.5 and 5%) were selected to balance aldehyde content and molecular weight reduction. For all the evaluated oxidation degrees, the process achieved a consistent and reproducible yield of approximately 74% and the real oxidation degrees closely matched the theoretical ones, confirming the high reaction conversion (Fig. 2A and Fig. S1A).[35,40,44] ATR-FTIR analysis also confirmed the successful oxidation of pectin, by detecting the characteristic absorbance bands associated with dialdehyde groups and -OH groups modifications (Fig. 2B and Fig. S1B).[32,42] As expected, PDA molecular weight decreased progressively with the increase of oxidation degrees, from 41 kDa for PDA_2.5 to 16 kDa for PDA_25, compared to the unmodified pectin (Fig. 2C and Fig. S1C).

In pectin hydrogels the presence of around 20 consecutive galacturonic acid rings is required for the formation of stable ionic junctions.[62] Hence, another side effect of oxidation is the opening of galacturonic acid rings, which weakens or even hinders ionic crosslinking.[62] Rheological analysis showed that ionic crosslinking ability of PDA using calcium ions decreased with increasing PDA oxidation degree. Indeed PDA_10 and PDA_25 were unable to undergo ionic crosslinking. In contrast, the PDA_2.5 and PDA_5 hydrogels could crosslink in the presence of $CaCl_2$, showing lower storage moduli (2956 Pa and 657 Pa, respectively) compared to unmodified pectin hydrogels

(3620 Pa) (Fig. 2D). Indeed, PDA_2.5 hydrogel showed a modest non-significant 1.2-fold reduction in Young's modulus compared to unmodified pectin hydrogels (11.8 kPa), while PDA_5 hydrogels exhibited a statistically significant 5.6-fold decrease (Fig. 2E).

The use of pectin hydrogels for DDS is mainly limited by their inherent acidifying effect, which can negatively affect cell viability and compatibility with biological applications. To mitigate this effect and stabilize the pH, various buffering agents can be employed, such as sodium hydroxide (NaOH), sodium bicarbonate (NaHCO$_3$) or other alkaline compounds.[28,31] Widely used NaOH can cause precipitation and degradation of poly(galacturonic acid) chains in pectin when exposed to alkaline conditions for extended periods.[28] Conversely, suitable concentrations of NaHCO$_3$ protonate the carboxyl groups of the PDA backbone while preventing β-elimination, allowing a pH increase without causing polysaccharide depolymerization.[28] An integrated approach involving NaHCO$_3$ and CaCO$_3$ was also proposed.[63] To increase the pH, PDA solutions (having a starting pH of ~3) can be brought to pH ~3.3 by dissolving PDA in 20 mM NaHCO$_3$. CaCO$_3$ enables internal pre-crosslinking by gradually dissolving in acidic environments, releasing calcium ions (Ca^{2+}) and carbonate ions (CO$_3^{2-}$). Calcium ions promote crosslinking through the formation of an "egg-box" structure between pectin molecules, while carbonate ions have a pH buffering effect, gradually raising the pH to near-physiological levels.[28,31] In this study, PDA pre-crosslinking was optimized by investigating two CaCO$_3$ low concentrations (20 and 30 mM) and two polymer concentrations (3% and 4%) to stabilize the pH without fully crosslinking the PDA solutions, thereby ensuring hydrogel injectability.[31] Hydrogels with 3% w/v concentration and 30 mM CaCO$_3$ reached physiological pH levels more rapidly (Fig. 2F). This result was validated by cytocompatibility assays (Fig. 2G), showing only slightly reduced cell viability with hydrogels crosslinked with 20 mM CaCO$_3$, likely due to lower pH levels.

To address the lack of cell-adhesive moieties of pectin hydrogels, several studies reported pectin aldehyde groups chemically crosslinked with gelatin through Schiff base formation.[33,34,54] However, imine bonds formed during this reaction are inherently unstable in aqueous environments, posing a challenge for long-term stability in physiological conditions. Nejati et al. recently developed an injectable hydrogel based on PDA combined with gelatin-graft-polypyrrole via Schiff base formation, enabling dynamic covalent bonding for injectability but exhibiting rapid degradation with a 60–80% weight loss within 14 days.[35] In this study, a preliminary investigation was conducted into the crosslinking dynamics of PDA/gelatin hydrogels by employing PDA hydrogels with 3% w/v concentration and 30 mM CaCO$_3$. Rheological data (Fig. S2A and B) showed that only hydrogels with the high PDA ratio (PDA:gelatin ratio of 70:30% w/w) formed stable structures at both physiological (37 °C) and room (25 °C) temperatures. Hydrazone bonds, formed by the reaction of hydrazides with aldehydes or ketones, are dynamic covalent bonds that exhibit

greater stability in aqueous environments, particularly at physiological pH, due to the presence of the nitrogen–nitrogen bonds.[64] Therefore, to improve the interaction between aldehyde groups in oxidized pectin and amino groups in gelatin, G-CDH was produced through a carbodiimide-mediated coupling reaction, functionalizing gelatin with carbohydrazide, achieving an average 37% degree of modification, similar to previous literature results,[36] with a high yield of production (92%) (Fig. 3A).[36,55] Previous reports have focused on using G-CDH with other oxidized polysaccharides, such as oxidized hyaluronic acid[36,37] and oxidized alginate.[38] This study represents the first one combining G-CDH and PDA to incorporate drug-loaded NPs within a hydrazone-crosslinked network, with the aim of developing stable, injectable, and self-healing hydrogels. Furthermore, the use of hydrazone bonds for crosslinking PDA has been explored in combination with poly(N-isopropylacrylamide)-bearing acyl hydrazide groups to get hydrogels for anticancer therapy.[65]

The crosslinking ability between PDA and G-CDH was thoroughly investigated by combining PDA_2.5 and PDA_5 (crosslinked with 30 mM CaCO$_3$) with G-CDH at three different PDA:G-CDH ratios (30:70, 50:50, and 70:30% w/w). Unlike PDA/gelatin hydrogels, which only formed at the highest PDA ratios, rheological analysis showed that PDA/G-CDH hydrogels were successfully obtained (G' higher than G'') at all the tested ratios, demonstrating their tunable rheological properties (Fig. 3B–D). PDA_5/G-CDH hydrogels exhibited the highest storage modulus (G'), reaching 115 Pa with the 50:50 composition, which corresponded to a Young's modulus of 342 Pa. On the other side, PDA_2.5/G-CDH (70:30) hydrogel showed the highest G' values among the PDA_2.5-based compositions, with a corresponding Young's modulus of 132 Pa. Stability tests further supported these findings: all hydrogel compositions displayed a decrease in wet weight over time, consistent with observations in the literature.[36,38]

However, among them, PDA_2.5/G-CDH (70:30) had the lowest degree of dissolution, followed closely by PDA_5/G-CDH (50:50) hydrogel (Fig. 3F). Based on these findings, PDA_2.5/G-CDH (70:30) and PDA_5/G-CDH (50:50) were identified as the most promising candidates for the sustained release of drug-loaded NPs over extended periods. Rheological and stability results were corroborated by TNBS assay data, which showed that these compositions achieved aldehyde-to-amine ratios close to 1, i.e., 0.86 for PDA_2.5/G-CDH (70:30) and 1.22 for PDA_5/G-CDH (50:50), consistent with effective crosslinking (Fig. 3E). Only one previous study explored similar ratios for G-CDH and oxidized hyaluronic acid (HA), reporting a G-CDH:HA ratio of around 1.1.[36] A nearly equivalent aldehyde-to-amine ratio enables a well-balanced interaction, resulting in an optimally crosslinked network that provides the necessary stability and mechanical properties to the resulting hydrogel.[66] Deviations from this ratio lead to the inability to stably retain one of the components in the hydrogel network, leading to decreased hydrogel structure and stability. Furthermore, any residual unreacted aldehydes may cause cytotoxic effects, as reported with oxidized alginate/gelatin

bioinks.[67] Furthermore, the aldehyde-to-amine ratio impacts not only the crosslinking density but also the dynamic behavior of the bonds, affecting properties such as self-healing.[59] The ability of the Schiff base bonds to break and reform, which is essential for self-healing, relies on an appropriate aldehyde-to-amine ratio. When the gel network is disrupted, the amino or hydrazide groups on the exposed surface rapidly interact with nearby aldehyde groups, forming new covalent bonds. Therefore, self-healing hydrogels require a balanced aldehyde-to-amine ratio for optimal performance, as shown by Heo *et al.*, who attributed the lack of self-healing in their oxidized alginate/G-CDH hydrogel to an imbalance in these groups.[38] The selected PDA_2.5/G-CDH (70 : 30) and PDA_5/G-CDH (50 : 50) hydrogels showed excellent sol-to-gel recovery ability (Fig. 4D). The hydrogels regained their mechanical integrity after high stress, confirming their suitability for injectable applications. Self-healing was visually confirmed by the reconnection of differently colored cut pieces of hydrogels, with PDA_2.5/G-CDH (70 : 30) hydrogel showing greater resistance to twisting and stretching compared to PDA_5/G-CDH (50 : 50) samples (Fig. 4E and F). Self-healing hydrogels offer significant advantages in DDSs by ensuring structural integrity after mechanical rupture and adapting to patient-specific defects.[67] Their gel–sol transition allows for smooth injection, precise localization and the formation of a sustained therapeutic depot, making them ideal for minimally invasive treatments targeting deep-seated lesions. Injectability tests demonstrated that PDA_2.5/G-CDH (70 : 30) and PDA_5/G-CDH (50 : 50) were easily injectable through needles with decreasing sizes from 20-G up to 27-G (Fig. 4A and B), thanks to the dynamic Schiff base bonds enabling reversible gel-to-sol transition. Rheological analysis confirmed their shear-thinning behavior, supporting their suitability for injectable applications (Fig. 4C).

Thus, the combination of PDA/G-CDH hydrogels with CurZNPs was investigated to develop novel hybrid NP/hydrogel DDS for the controlled release of curcumin *in situ*, for local antioxidant therapies. The curcumin release profile was evaluated, demonstrating the enhanced ability of the hydrogels to provide a sustained release of curcumin when encapsulated in CurZNPs (Fig. 6A). Compared to Cur-loaded hydrogels, which completed their release within approximately 7 days, CurZNPs-loaded hydrogels extended the release period to 28 days. DLS analyses confirmed the release of CurZNPs, with average sizes ranging from 200 to 270 nm, supporting the potential for sustained CurZNPs release and subsequent cellular internalization (Table S1 and Fig. S3). Kinetic modelling using the Ritger–Peppas equation further confirmed that CurZNPs-loaded PDA/G-CDH hydrogels effectively modulate curcumin transport, shifting the release from a rapid diffusion-dominated profile for CurZNPs to a profile governed by both diffusion and matrix relaxation (Table 4).[56] The reduced kinetic constant k observed for the hybrid DDSs indicates that CurZNPs confinement within the hydrogel mesh introduces an additional diffusion barrier, resulting in slower and more sustained release.[57] This behavior is consistent with the pro-

longed release observed experimentally and is particularly relevant for the treatment of chronic and prolonged tissue inflammation.[68] Therefore, Cur-loaded hydrogels may not provide enough time to support comprehensive tissue healing. Furthermore, as hydrazone linkages are known to retain stability at physiological pH while degrading more rapidly in mildly acidic microenvironments, it would be particularly interesting in future studies to assess whether this chemistry could contribute to pH-responsive modulation of curcumin release in acidic microenvironments typical of inflamed or injured tissues.[65] Among the formulations, PDA_2.5/G-CDH (70 : 30) hydrogel exhibited the most sustained release within 21 days, thus offering a more effective and consistent solution, making it the optimal candidate for further *in vitro* studies.

To mimic oxidative stress conditions, we first determined the appropriate concentration of H_2O_2 to induce oxidative stress in HFF-1 cells. HFF-1 cells were affected by H_2O_2 treatment with increasing H_2O_2 concentration, as already reported in the previous literature (Fig. 6B).[2,48] Treatment with 0.8 and 1 mM of H_2O_2 significantly decreased cell viability to 63 and 44%, respectively, confirming its ability to induce cytotoxic damage. A viability threshold of ~60% was selected as appropriate for assessing antioxidant activity, as it represents a level of cellular stress from which cells can still recover.[2] The effect of curcumin on HFF-1 cells was subsequently assessed, showing that concentrations up to 5 µg mL^{-1} did not significantly affect cell viability (Fig. 6C). To assess curcumin protective effects against oxidative damage, HFF-1 cells were pretreated for 7 days with CurZNPs-loaded PDA_2.5/G-CDH (70 : 30) hydrogels to ensure consistent curcumin release. Pretreatment with CurZNPs-loaded hydrogels effectively reversed the damage caused by H_2O_2 treatment by restoring cell viability to levels comparable to untreated cells. Notably, this protective effect was more pronounced compared to Cur-loaded PDA_2.5/G-CDH (70 : 30) hydrogels or CurZNPs alone (Fig. 6D). Cur-loaded hydrogels also showed partial recovery of viability, likely due to a higher release of curcumin at each time point compared to CurZNPs-loaded hydrogels and lower cell uptake. The obtained results suggested that longer culture times will highlight the beneficial effects of CurZNPs-loaded PDA_2.5/G-CDH (70 : 30) hydrogels, maintaining curcumin availability for extended antioxidant protection compared to Cur-loaded ones, which were only effective at short time points.

Moreover, the anti-inflammatory potential of CurZNPs was examined using RAW 264.7 macrophages to assess whether the sustained release offered by the PDA_2.5/G-CDH (70 : 30) hydrogel could enhance the therapeutic response. CurZNPs released from the hydrogel significantly reduced NO production in LPS-stimulated cells compared with free CurZNPs, demonstrating a stronger and prolonged anti-inflammatory effect (Fig. 7A). Immunofluorescence staining supported these results, showing a clear decrease in CD86 expression in cells seeded onto CurZNPs-loaded PDA_2.5/G-CDH (70 : 30) hydrogels, whereas free CurZNPs induced only a partial reduction (Fig. 7B). This further confirms that the hybrid DDS enhances

curcumin availability over time and more effectively suppresses macrophage activation, underscoring its potential for localized anti-inflammatory therapies.

In conclusion, the results suggest that PDA_2.5/G-CDH hydrogels are highly effective for the *in situ* delivery of CurZNPs, making them a promising solution for antioxidant therapies. These hydrogels enable the localized, sustained release of CurZNPs and also contribute to keeping the bioactivity of curcumin, which is crucial for mitigating oxidative stress at the target site and promoting soft tissue repair. The combination of the dynamic Schiff-base bonds in the hydrogel structure and encapsulated CurZNPs provides a dual benefit of structural support and therapeutic delivery, highlighting the potential of this system in advanced soft tissue care. This innovative approach aims to address the challenges of delivering hydrophobic drugs within hydrogels, minimizing systemic side effects and enabling a prolonged and site-specific effect.

CurZNPs-loaded PDA/G-CDH hydrogels represent the first reported combination of G-CDH and PDA to get stable, injectable, and self-healing hydrogels for controlled and sustained CurZNPs delivery for efficient antioxidant therapy.

In the future, focusing on clinical therapeutic markers, such as those specific to wound healing, longer culture periods and a wider variety of cell lines, will be crucial in evaluating the effectiveness of this system for the targeted delivery of antioxidant treatments across various clinical applications. Deeper investigations will help to better understand the full potential of this DDS in addressing diverse therapeutic needs, particularly in antioxidant and anti-inflammatory treatment scenarios. Preliminary cytocompatibility studies demonstrated high cell viability for PDA_5/G-CDH (50 : 50) and PDA_2.5/G-CDH (70 : 30) hydrogel formulations up to day 7, highlighting the beneficial effects of both $CaCO_3$ crosslinking and the addition of G-CDH (Fig. 5A). The beneficial effect of G-CDH was further demonstrated by the complete colonization of the hydrogel surfaces with cells after 7 days of culture. This was attributed to the G-CDH cell-adhesive moieties, such as RGD sequences, which are known to promote integrin-mediated cell adhesion (Fig. 5B). Notably, both hydrogels supported high cell proliferation, with cells exhibiting a well-spread morphology. These findings not only validate DDS cytocompatibility but also provide valuable insights for designing cell-laden hydrogels tailored to specific therapeutic needs, such as for bioprinting applications. By leveraging this platform, future advancements in sustainable and precise DDS could significantly enhance regenerative medicine and tissue engineering strategies.

5. Conclusions

In this study, our ambition was to exploit sustainable natural-derived polymers to address one major challenge in local therapeutic strategies, *i.e.*, the need for effective, safe DDSs. Pectin and zein were selected as biomaterials for hydrogel and NP preparation, respectively. We prepared sustainable and efficient CurZNPs for curcumin delivery and loaded them into injectable PDA/G-CDH hydrogels to achieve safe and controlled drug release.

To develop injectable hydrogels, pectin was oxidized to introduce reactive aldehyde groups and blended with G-CDH, to form chemically-crosslinked hydrogels, with physical pre-crosslinking achieved using $CaCO_3$. Two compositions, PDA_2.5/G-CDH (70 : 30) and PDA_5/G-CDH (50 : 50), were selected for their tunable rheological properties, injectability, self-healing and cytocompatibility. CurZNPs were produced *via* nanoprecipitation, to minimize the use of organic solvents: they showed high encapsulation efficiency and antioxidant activity. Embedding CurZNPs into hydrogels allowed sustained curcumin release, particularly for the PDA_2.5/G-CDH (70 : 30) formulation. Therapeutic efficacy of the final NPs-hydrogel DDS was confirmed by restoring HFF-1 viability after oxidative stress and assessing reduced NO production in RAW 264.7 cells after induced inflammation.

Overall, the results demonstrated that PDA_2.5/G-CDH (70 : 30) hydrogels are suitable for *in situ* delivery of CurZNPs. Future investigations at longer times and using other cell lines will evaluate the ability of the designed DDS for controlled and sustained antioxidant treatment in different clinical applications, paving the way towards innovative and efficient DDSs for antioxidant and anti-inflammatory therapies.

Author contributions

The manuscript was written through contributions of all authors. All authors have given approval to the final version of the manuscript. F. T.: investigation, methodology, validation, data analysis, and writing––original draft; E. M.: investigation, methodology, validation, data analysis, writing––review and editing; C.P.: investigation, methodology, validation, data analysis; A. Z.: investigation, methodology, validation, data analysis; I. C.: supervision (co-supervision of F. Tivano, PhD student activity), conceptualization, and writing––review and editing; C. M: supervision (co-supervision of F. Tivano, PhD student activity), conceptualization, and writing––review and editing; V. C.: supervision (project supervision; co-supervision of F. Tivano PhD student activity); conceptualization; writing––review and editing, project administration, resources, and funding acquisition.

Conflicts of interest

There are no conflicts to declare.

Data availability

The data supporting this article are openly available in the Zenodo repository at 10.5281/zenodo.18662040.

Supplementary information (SI): PDA_5 and PDA_25 synthesis and characterizations (synthesis parameters, yields of

productions, real oxidation degree values, FTIR spectra and the ability of PDA to crosslink with calcium ions). PDA/gelatin hydrogel rheological tests; DLS analyses of CurZNPs release from PDA/G-CDH hydrogels. See DOI: https://doi.org/10.1039/d5bm01302j.

Acknowledgements

References

1 W. Zhang, L. Chen, Y. Xiong, A. C. Panayi, A. Abududilibaier, Y. Hu, et al., Antioxidant Therapy and Antioxidant-Related Bionanomaterials in Diabetic Wound Healing, *Front. Bioeng. Biotechnol.*, 2021, **9**, 707479, DOI: 10.3389/FBIOE.2021.707479.

2 W. Hu, J. Zhang, H. Wang, M. Guan, L. Dai, J. Li, et al., Protective effects of isorhamnetin against H_2O_2-induced oxidative damage in HaCaT cells and comprehensive analysis of key genes, *Sci. Rep.*, 2023, **13**, 2498, DOI: 10.1038/s41598-023-27575-7.

3 X. Chen, Y. Zhang, W. Yu, W. Zhang, H. Tang and W. E. Yuan, In situ forming ROS-scavenging hybrid hydrogel loaded with polydopamine-modified fullerene nanocomposites for promoting skin wound healing, *J. Nanobiotechnol.*, 2023, **21**(1), 1–15, DOI: 10.1186/s12951-023-01879-2.

4 H. J. Forman and H. Zhang, Targeting oxidative stress in disease: promise and limitations of antioxidant therapy, *Nat. Rev. Drug Discovery*, 2021, **20**(9), 689–709, DOI: 10.1038/s41573-021-00233-1.

5 D. Monti, S. Tampucci, R. Tiwari and K. Pathak, Local Drug Delivery Strategies towards Wound Healing, *Pharmaceutics*, 2023, **15**(2), 634, DOI: 10.3390/PHARMACEUTICS15020634.

6 I. M. Comino-Sanz, M. D. López-Franco, B. Castro and P. L. Pancorbo-Hidalgo, The Role of Antioxidants on Wound Healing: A Review of the Current Evidence, *J. Clin. Med.*, 2021, **10**(16), 3558, DOI: 10.3390/jcm10163558.

7 B. Kumar, R. Aggarwal, U. Prakash and P. K. Sahoo, Emerging therapeutic potential of curcumin in the management of dermatological diseases: an extensive review of drug and pharmacological activities, *Future J. Pharm. Sci.*, 2023, **9**(1), 1–10, DOI: 10.1186/s43094-023-00493-1.

8 A. Kumari, N. Raina, A. Wahi, K. W. Goh, P. Sharma, R. Nagpal, et al., Wound-Healing Effects of Curcumin and Its Nanoformulations: A Comprehensive Review, *Pharmaceutics*, 2022, **14**(11), 2288, DOI: 10.3390/PHARMACEUTICS14112288.

9 Y. Dong and Z. Wang, ROS-scavenging materials for skin wound healing: advancements and applications, *Front. Bioeng. Biotechnol.*, 2023, **11**, 1304835, DOI: 10.3389/fbioe.2023.1304835.

10 Z. Sohani, S. Jamshidi, M. K. Koohi, J. Malakootikhah, M. Abarkar, D. Golchin, et al., Novel ophthalmic hyaluronic acid-hydrogel with curcumin nanoparticles for enhanced healing of ulcerative keratitis in rabbit model, *Sci. Rep.*, 2024, **14**(1), 23046, DOI: 10.1038/S41598-024-74195-W.

11 J. Liu, Z. Chen, J. Wang, R. Li, T. Li, M. Chang, et al., Encapsulation of Curcumin Nanoparticles with MMP9-Responsive and Thermos-Sensitive Hydrogel Improves Diabetic Wound Healing, *ACS Appl. Mater. Interfaces*, 2018, **10**(19), 16315–16326, DOI: 10.1021/acsami.8b03868.

12 W. Choi and D. S. Kohane, Hybrid Nanoparticle-Hydrogel Systems for Drug Delivery Depots and Other Biomedical Applications, *ACS Nano*, 2024, **18**(34), 22780–22792, DOI: 10.1021/acsnano.4c06888.

13 D. T. Pham, K. Navesit, L. Wiwatkunupakarn, P. Chomchalao and W. Tiyaboonchai, Nanoparticles-hydrogel composites: A promising innovative system for local antimicrobial applications, *J. Drug Deliv. Sci. Technol.*, 2023, **89**, 105055, DOI: 10.1016/j.jddst.2023.105055.

14 F. Tivano and V. Chiono, Zein as a renewable material for the preparation of green nanoparticles for drug delivery, *Front. Biomater. Sci.*, 2023, **2**, 1156403, DOI: 10.3389/fbiom.2023.1156403.

15 S. Tortorella, M. Maturi, V. Vetri Buratti, G. Vozzolo, E. Locatelli, L. Sambri, et al., Zein as a versatile biopolymer: different shapes for different biomedical applications, *RSC Adv.*, 2021, **11**(62), 39004–39026, DOI: 10.1039/d1ra07424e.

16 Q. Liu, Y. Jing, C. Han, H. Zhang and Y. Tian, Encapsulation of curcumin in zein/caseinate/sodium alginate nanoparticles with improved physicochemical and controlled release properties, *Food Hydrocolloids*, 2019, **93**, 432–442, DOI: 10.1016/j.foodhyd.2019.02.003.

17 S. Podaralla and O. Perumal, Influence of formulation factors on the preparation of zein nanoparticles, *AAPS PharmSciTech*, 2012, **13**(3), 919–927, DOI: 10.1208/s12249-012-9816-1.

18 K. Yao, W. Chen, F. Song, D. J. McClements and K. Hu, Tailoring zein nanoparticle functionality using biopolymer coatings: Impact on curcumin bioaccessibility and antioxidant capacity under simulated gastrointestinal conditions, *Food Hydrocolloids*, 2018, **79**, 262–272, DOI: 10.1016/j.foodhyd.2017.12.029.

19 S. Chen, Q. Li, D. J. McClements, Y. Han, L. Dai, L. Mao, *et al.*, Co-delivery of curcumin and piperine in zein-carrageenan core-shell nanoparticles: Formation, structure, stability and in vitro gastrointestinal digestion, *Food Hydrocolloids*, 2020, **99**, 105334, DOI: 10.1021/acsami.9b11782.

20 M. F. M. A. Zamri, R. Bahru, R. Amin, M. U. A. Khan, S. I. A. Razak, S. A. Hassan, *et al.*, Waste to health: A review of waste derived materials for tissue engineering, *J. Cleaner Prod.*, 2021, **290**, 125792, DOI: 10.1016/j.jclepro.2021.125792.

21 FAO. *Citrus Fruit Fresh And Processed Statistical bulletin 2020*. 2021. Available from: https://www.fao.org/economic/est/est-commodities/citrus-fruit/en/.

22 V. Vancauwenberghe, M. A. Delele, J. Vanbiervliet, W. Aregawi, P. Verboven, J. Lammertyn, *et al.*, Model-based design and validation of food texture of 3D printed pectin-based food simulants, *J. Food Eng.*, 2018, **231**, 72–82, DOI: 10.1016/j.jclepro.2021.125792.

23 A. Roman-Benn, C. A. Contador, M. W. Li, H. M. Lam, K. Ah-Hen, P. E. Ulloa, *et al.*, Pectin: An overview of sources, extraction and applications in food products, biomedical, pharmaceutical and environmental issues, *Food Chem. Adv.*, 2023, **2**, 100192, DOI: 10.1016/J.FOCHA.2023.100192.

24 C. E. Campiglio, A. Carcano and L. Draghi, RGD-pectin microfiber patches for guiding muscle tissue regeneration, *J. Biomed. Mater. Res., Part A*, 2022, **110**(3), 515–524, DOI: 10.1002/JBM.A.37301.

25 P. Jantrawut, J. Bunrueangtha, J. Suerthong and N. Kantrong, Fabrication and characterization of low methoxyl pectin/gelatin/carboxymethyl cellulose absorbent hydrogel film for wound dressing applications, *Materials*, 2019, **12**, 1628, DOI: 10.3390/ma12101628.

26 C. Lara-Espinoza, E. Carvajal-Millán, R. Balandrán-Quintana, Y. López-Franco and A. Rascón-Chu, Pectin and Pectin-Based Composite Materials: Beyond Food Texture, *Molecules*, 2018, **23**, 942, DOI: 10.3390/molecules23040942.

27 C. Hu, W. Lu, A. Mata, K. Nishinari and Y. Fang, Ions-induced gelation of alginate: Mechanisms and applications, *Int. J. Biol. Macromol.*, 2021, **177**, 578–588, DOI: 10.1016/J.IJBIOMAC.2021.02.086.

28 H. R. Moreira, F. Munarin, R. Gentilini, L. Visai, P. L. Granja, M. C. Tanzi, *et al.*, Injectable pectin hydrogels produced by internal gelation: PH dependence of gelling and rheological properties, *Carbohydr. Polym.*, 2014, **103**(1), 339–347, DOI: 10.1016/j.carbpol.2013.12.057.

29 L. Zhang, J. Zheng, Y. Wang, X. Ye, S. Chen, H. Pan, *et al.*, Fabrication of rhamnogalacturonan-I enriched pectin-based emulsion gels for protection and sustained release

of curcumin, *Food Hydrocolloids*, 2022, **128**, 107592, DOI: 10.1016/J.FOODHYD.2022.107592.

30 R. Cai, S. Pan, R. Li, X. Xu, S. Pan and F. Liu, Curcumin loading and colon release of pectin gel beads: Effect of different de-esterification method, *Food Chem.*, 2022, **389**, 133130, DOI: 10.1016/J.FOODCHEM.2022.133130.

31 M. Merli, L. Sardelli, N. Baranzini, A. Grimaldi, E. Jacchetti, M. T. Raimondi, *et al.*, Pectin-based bioinks for 3D models of neural tissue produced by a pH-controlled kinetics, *Front. Bioeng. Biotechnol.*, 2022, **10**, 1032542, DOI: 10.3389/fbioe.2022.1032542.

32 B. Gupta, M. Tummalapalli, B. L. Deopura and M. S. Alam, Functionalization of pectin by periodate oxidation, *Carbohydr. Polym.*, 2013, **98**(1), 1160–1165, DOI: 10.1016/j.carbpol.2013.06.069.

33 A. Chetouani, M. Elkolli, H. Haffar, H. Chader, F. Riahi, T. Varacavoudin, *et al.*, Multifunctional hydrogels based on oxidized pectin and gelatin for wound healing improvement, *Int. J. Biol. Macromol.*, 2022, **212**, 248–256, DOI: 10.1016/j.ijbiomac.2022.05.082.

34 C. A. Garrido, M. Vargas and J. F. Alvarez-Barreto, Auto-cross-linking hydrogels of hydrogen peroxide-oxidized pectin and gelatin for applications in controlled drug delivery, *Int. J. Polym. Sci.*, 2019, **2019**, DOI: 10.1155/2019/9423565.

35 S. Nejati, R. K. Soflou, S. Khorshidi and A. Karkhaneh, Development of an oxygen-releasing electroconductive *in situ* crosslinkable hydrogel based on oxidized pectin and grafted gelatin for tissue engineering applications, *Colloids Surf., B*, 2020, **196**, DOI: 10.1016/j.colsurfb.2020.111347.

36 T. Hozumi, T. Kageyama, S. Ohta, J. Fukuda and T. Ito, Injectable Hydrogel with Slow Degradability Composed of Gelatin and Hyaluronic Acid Cross-Linked by Schiff's Base Formation, *Biomacromolecules*, 2018, **19**(2), 288–297, DOI: 10.1021/acs.biomac.7b01133.

37 L. L. Wang, C. B. Highley, Y. C. Yeh, J. H. Galarraga, S. Uman and J. A. Burdick, Three-dimensional extrusion bioprinting of single- and double-network hydrogels containing dynamic covalent crosslinks, *J. Biomed. Mater. Res., Part A*, 2018, **106**(4), 865–875, DOI: 10.1002/jbm.a.36323.

38 D. N. Heo, M. A. Alioglu, Y. Wu, V. Ozbolat, B. Ayan, M. Dey, *et al.*, 3D Bioprinting of Carbohydrazide-Modified Gelatin into Microparticle-Suspended Oxidized Alginate for the Fabrication of Complex-Shaped Tissue Constructs, *ACS Appl. Mater. Interfaces*, 2020, **12**(18), 20295–20306, DOI: 10.1021/acsami.0c05096.

39 A. Chetouani, N. Follain, S. Marais, C. Rihouey, M. Elkolli, M. Bounekhel, *et al.*, Physicochemical properties and biological activities of novel blend films using oxidized pectin/chitosan, *Int. J. Biol. Macromol.*, 2017, **97**, 348–356, DOI: 10.1016/j.ijbiomac.2017.01.018.

40 B. Sarker, D. G. Papageorgiou, R. Silva, T. Zehnder, F. Gul-E-Noor, M. Bertmer, *et al.*, Fabrication of alginate–gelatin crosslinked hydrogel microcapsules and evaluation of the microstructure and physico-chemical properties, *J. Mater. Chem. B*, 2014, **2**(11), 1470–1482, DOI: 10.1039/C3TB21509A.

41 D. q. Li, S. y. Wang, Y. j. Meng, J. f. Li and J. Li, An injectable, self-healing hydrogel system from oxidized pectin/chitosan/γ-Fe2O3, *Int. J. Biol. Macromol.*, 2020, **164**, 4566–4574, DOI: 10.1016/J.IJBIOMAC.2020.09.072.

42 H. Wang, X. Chen, Y. Wen, D. Li, X. Sun, Z. Liu, *et al.*, A Study on the Correlation between the Oxidation Degree of Oxidized Sodium Alginate on Its Degradability and Gelation, *Polymers*, 2022, **14**, 1679, DOI: 10.3390/polym14091679.

43 X. Huang, X. Huang, Y. Gong, H. Xiao, D. J. Mcclements and K. Hu, Enhancement of Curcumin Water Dispersibility and Antioxidant Activity using Core-shell Protein-polysaccharide Nanoparticles, *Food Res. Int.*, 2016, **87**, 1–9, DOI: 10.1016/j.foodres.2016.06.009.

44 F. Munarin, P. Petrini, M. C. Tanzi, M. A. Barbosa and P. L. Granja, Biofunctional chemically modified pectin for cell delivery, *Soft Matter*, 2012, **8**(17), 4731–4739, DOI: 10.1039/c2sm07260b.

45 G. Kaklamani, D. Cheneler, L. M. Grover, M. J. Adams and J. Bowen, Mechanical properties of alginate hydrogels manufactured using external gelation, *J. Mech. Behav. Biomed. Mater.*, 2014, **36**, 135–142, DOI: 10.1016/J.JMBBM.2014.04.013.

46 R. A. Suhar, V. M. Doulames, Y. Liu, M. E. Hefferon, O. Figueroa, H. Buabbas, *et al.*, Hyaluronan and elastin-like protein (HELP) gels significantly improve microsphere retention in the myocardium, *Biomater. Sci.*, 2022, **10**, 2590–2608, DOI: 10.1039/d1bm01890f.

47 M. Caprioli, I. Roppolo, A. Chiappone, L. Larush, C. F. Pirri and S. Magdassi, 3D-printed self-healing hydrogels via Digital Light Processing, *Nat. Commun.*, 2021, **12**, 2462, DOI: 10.1038/s41467-021-22802-z.

48 W. H. Park, Effects of antioxidants and MAPK inhibitors on cell death and reactive oxygen species levels in H_2O_2-treated human pulmonary fibroblasts, *Oncol. Lett.*, 2013, **5**(5), 1633–1638, DOI: 10.3892/ol.2013.1216.

49 T. Zhang, S. Yu, X. Tang, C. Ai, H. Chen, J. Lin, *et al.*, Ethanol-soluble polysaccharide from sugar beet pulp for stabilizing zein nanoparticles and improving encapsulation of curcumin, *Food Hydrocolloids*, 2022, **124**, 107208, DOI: 10.1016/j.foodhyd.2021.107208.

50 M. Colaço, T. Roquito, J. P. Costa, M. T. Cruz and O. Borges, The Effect of Curcumin-Loaded Glucan Nanoparticles on Immune Cells: Size as a Critical Quality Attribute, *Pharmaceutics*, 2023, **15**(2), 623, DOI: 10.3390/PHARMACEUTICS15020623.

51 Y. Huang, B. S. B. Canup, S. Gou, N. Chen, F. Dai, B. Xiao, *et al.*, Oral nanotherapeutics with enhanced mucus penetration and ROS-responsive drug release capacities for delivery of curcumin to colitis tissues, *J. Mater. Chem. B*, 2021, **9**(6), 1604–1615, DOI: 10.1039/D0TB02092C.

52 G. M. Pontes-Quero, L. Benito-Garzón, J. P. Cano, M. R. Aguilar and B. Vázquez-Lasa, Amphiphilic polymeric nanoparticles encapsulating curcumin: Antioxidant, anti-inflammatory and biocompatibility studies, *Mater. Sci. Eng., C*, 2021, **121**, 111793, DOI: 10.1016/J.MSEC.2020.111793.

53 M. Li, Q. Hou, L. Zhong, Y. Zhao and X. Fu, Macrophage Related Chronic Inflammation in Non-Healing Wounds, *Front. Immunol.*, 2021, **12**, 681710, DOI: 10.3389/FIMMU.2021.681710.

54 A. Chetouani, M. Elkolli, M. Bounekhel and D. Benachour, Synthesis and properties of novel hydrogels from oxidized pectin crosslinked gelatin for biomedical applications, *Polym. Bull.*, 2014, **71**(9), 2303–2316, DOI: 10.1007/s00289-014-1189-z.

55 Y. Zhang, X. Li, N. Zhong, Y. Huang, K. He and X. Ye, Injectable in situ dual-crosslinking hyaluronic acid and sodium alginate based hydrogels for drug release, *J. Biomater. Sci., Polym. Ed.*, 2019, **30**(12), 995–1007, DOI: 10.1080/09205063.2019.1618546.

56 J. Li and D. J. Mooney, Designing hydrogels for controlled drug delivery, *Nat. Rev. Mater.*, 2016, **1**(12), 1–17, DOI: 10.1038/natrevmats.2016.71.

57 S. Shukla and A. Shukla, Tunable antibiotic delivery from gellan hydrogels, *J. Mater. Chem. B*, 2018, **6**(40), 6444–6458, DOI: 10.1039/C8TB00980E.

58 H. Fei, Y. Qian, T. Pan, Y. Wei and Y. Hu, Curcumin alleviates hypertrophic scarring by inhibiting fibroblast activation and regulating tissue inflammation, *J. Cosmet. Dermatol.*, 2024, **23**(1), 227–235, DOI: 10.1111/jocd.15905.

59 S. Shekhar, V. Chaudhary, B. Sharma, A. Kumar, A. K. Bhagi and K. P. Singh, Sustainable Polysaccharide Hydrogels Based on Dynamic Schiff Base Linkages as Versatile Building Blocks for Fabricating Advanced Functional Materials, *J. Polym. Environ.*, 2022, **31**(4), 1257–1278, DOI: 10.1007/S10924-022-02685-X.

60 C. J. Cheng, M. Ferruzzi and O. G. Jones, Fate of lutein-containing zein nanoparticles following simulated gastric and intestinal digestion, *Food Hydrocolloids*, 2019, **87**, 229–236, DOI: 10.1016/j.foodhyd.2018.08.013.

61 F. Ullm, P. Riedl, A. Machado de Amorim, A. Patzschke, R. Weiß, S. Hauschildt, *et al.*, 3D Scaffold-Based Macrophage Fibroblast Coculture Model Reveals IL-10 Dependence of Wound Resolution Phase, *Adv. Biosyst.*, 2020, **4**(1), 1900220, DOI: 10.1002/ADBI.201900220.

62 F. Munarin, M. C. Tanzi and P. Petrini, Advances in biomedical applications of pectin gels, *Int. J. Biol. Macromol.*, 2012, **51**, 681–689, DOI: 10.1016/j.ijbiomac.2012.07.002.

63 E. Secchi, F. Munarin, M. D. Alaimo, S. Bosisio, S. Buzzaccaro, G. Ciccarella, *et al.*, External and internal gelation of pectin solutions: Microscopic dynamics versus macroscopic rheology, *J. Phys.: Condens. Matter*, 2014, **26**, 464106, DOI: 10.1088/0953-8984/26/46/464106.

64 L. S. Lisboa, M. Riisom, H. J. Dunne, D. Preston, S. M. F. Jamieson, L. J. Wright, *et al.*, Hydrazone- and imine-containing [PdPtL4]4 + cages: a comparative study of the stability and host–guest chemistry, *Dalton Trans.*, 2022, **51**(48), 18438–18445, DOI: 10.1039/D2DT02720H.

65 H. An, Y. Yang, Z. Zhou, Y. Bo, Y. Wang, Y. He, *et al.*, Pectin-based injectable and biodegradable self-healing hydrogels for enhanced synergistic anticancer therapy, *Acta Biomater.*, 2021, **131**, 149–161, DOI: 10.1016/J.ACTBIO.2021.06.029.

66 J. Xu, Y. Liu and S. h. Hsu, Hydrogels Based on Schiff Base Linkages for Biomedical Applications, *Molecules*, 2019, **24**(16), 3005, DOI: 10.3390/MOLECULES24163005.

67 U. S. Malik, M. B. K. Niazi, Z. Jahan, M. I. Zafar, D. V. N. Vo and F. Sher, Nano-structured dynamic Schiff base cues as robust self-healing polymers for biomedical and tissue engineering applications: a review, *Environ. Chem. Lett.*, 2021, **20**(1), 495–517, DOI: 10.1007/S10311-021-01337-1.

68 B. L. Patenall, K. A. Carter and M. R. Ramsey, Kick-Starting Wound Healing: A Review of Pro-Healing Drugs, *Int. J. Mol. Sci.*, 2024, **25**(2), 1304, DOI: 10.3390/IJMS25021304.